BEST AVAILABLE IMAGES

Defective images within this document are accurate representations of the original documents submitted by the applicant.

Defects in the images may include (but are not limited to):

- BLACK BORDERS
- TEXT CUT OFF AT TOP, BOTTOM OR SIDES
- FADED TEXT
- ILLEGIBLE TEXT
- SKEWED/SLANTED IMAGES
- COLORED PHOTOS
- BLACK OR VERY BLACK AND WHITE DARK PHOTOS
- GRAY SCALE DOCUMENTS

IMAGES ARE BEST AVAILABLE COPY.

As rescanning documents *will not* correct images, please do not report the images to the Image Problem Mailbox.

Remarks

The Examiner's indication that all of the items listed in the Information Disclosure Statements submitted to date have been considered, is acknowledged and much appreciated.

The Examiner's indication on the record that Claims 27-36 and Claims 45-52 are withdrawn from consideration by virtue of the Examiner's imposition of restriction and election of species requirements, and that Claims 37-44 are currently under consideration, is also acknowledged and appreciated.

Claims 37-44 have been cancelled. Claims 53-60 have been added. Each of Claims 53, 54 and 56-60 sets forth subject matter of the claim in different or better form that that of its former counterpart Claims 37, 38, and 40-44, respectively, by incorporating what was previously implicit in the counterpart claim and removing various terms, for example. Each of Claims 53, 54 and 56-60 is no narrower than its respective counterpart claim. Claim 55 has no former counterpart claim. No new matter has been added by virtue of the amendment to the claims.

The amendment of December 2, 2003 has been rejected under 35 U.S.C. 132 because it allegedly introduces new matter into the disclosure. In this rejection, the Examiner alleges that the replacement paragraph for page 6, lines 14-21 is considered to be new matter. The rejection is respectfully traversed.

The replacement paragraph for page 6, lines 14-21 from the Amendment of December 2, 2003 has been cancelled and a new replacement paragraph for page 6, lines 14-21 has been added. The new replacement paragraph, much like the now-cancelled paragraph, is reproduced below, in marked form to show the changes that were made relative to the original paragraph on page 6, lines 14-21. In the reproduction below, the replacement paragraph is also marked with superscript numbers to identify various instances of underlined text.

> The medium 15 includes porous matrix, and the porous matrix includes a metal organic, or metalorganic,[1] polymer, such as a photopolymer, wherein the term metal organic, or metalorganic, refers to a material that comprises an organic ligand attached to a metal atom or a metalloid atom.[2] (See Brinker, C. Jeffrey, et al., Sol-Gel Science, The Physics and Chemistry of Sol-Gel Processing, p. 2 (1990).)[3] A precursor of the polymer may be a metal alkoxide, ~~such as a silane~~ wherein the term metal alkoxide refers to a metal organic, or metalorganic, material, that has a metal-oxygen-carbon linkage or metalloid-oxygen-carbon linkage.[4] (Id.)[5] Herein, where "metal" is used in connection with a metal organic, or metalorganic, material, or in connection with a metal alkoxide, it encompasses metals and metalloids.[6] The metal or metalloid[7] may be aluminum, barium, antimony, calcium, chromium, copper, erbium, germanium, iron, lead, lithium, phosphorus, potassium, silicon,

tantalum, tin, titanium, vanadium, zinc, or zirconium. The precursor may include a photoactive group, such as methacrylate. In one embodiment, the precursor may be trimethoxysilypropyl methacrylate, also known as methacryloxypropyltrimethoxy silane.

Clearly, all of the subject matter that is not underlined in the replacement paragraph is original subject matter, and is thus unobjectionable. As to the underlined subject matter, it is submitted that same is merely a rephrasing of the original subject matter or an inclusion of dictionary or art-recognized definitions known at the time of filing of the application, as further demonstrated below, and is thus unobjectionable. See MPEP 2163.07.

As to the first instance of underlined text, it is submitted that at the time the present application was filed, it was known that the metal organic, metalorganic, and even metal-organic terminology were used interchangeably. Submitted herewith are four articles that predated the filing of the present application, three of which demonstrate the interchangeable use of metal organic and metalorganic and the remaining article demonstrating the interchangeable use of metal-organic and metalorganic. No new matter has been added to the present application by reference to this known usage.

As to the second instance of underlined text, it is submitted that at the time the present application was filed, it was known that such when such terminology was used in connection with a material it referred to a material that comprises an organic ligand attached to a metal atom or a metalloid atom. This is demonstrated by text from Brinker, C. Jeffrey, *et al.*, *Sol-Gel Science, The Physics and Chemistry of Sol-Gel Processing*, p. 2 (1990), a copy of which was submitted with the Amendment of December 2, 2003. Another copy of this text is submitted herewith, along with a copy of an inside page thereof that identifies the publication date of 1990. This text predated the filing of the present application. As to the third instance of underlined text, it simply refers to the above-mentioned text of Brinker *et al.* No new matter has been added to the present application by reference to this known usage and a source therefor. Additionally, it is clear that the above-mentioned text is consistent with the examples of metal organic or metalorganic materials provided in the original application, such as metal organic or metalorganic materials that may comprise any of the possible metals or metalloids, as set forth in the original text above, merely by way of example.

As to the fourth instance of underlined text, it is submitted that at the time the present application was filed, it was known that the term metal alkoxide referred to a metal organic or metalorganic material that has a metal-oxygen-carbon linkage or metalloid-oxygen-carbon linkage. This is demonstrated by text from the above-mentioned Brinker, C. Jeffrey, *et al.*,

Sol-Gel Science, The Physics and Chemistry of Sol-Gel Processing, p. 2 (1990). This text predated the filing of the present application. As to the fifth instance of underlined text, it simply refers to the above-mentioned text of Brinker *et al.* No new matter has been added to the present application by reference to this known usage and a source therefor. Additionally, it is clear that the above-referenced text is consistent with the examples of metal alkoxides provided in the original application, such as metal alkoxides that may comprise any of the possible metals or metalloids, as set forth in the original text above, merely by way of example.

As to the sixth instance of underlined text, it is submitted that at the time the present application was filed, it was known that the term "metal," when used in relation to metal organic or metalorganic materials and metal alkoxides, referred to both metals and metalloids. This is demonstrated by text from the above-mentioned Brinker, C. Jeffrey, *et al.*, *Sol-Gel Science, The Physics and Chemistry of Sol-Gel Processing*, p. 2 (1990). This text predated the filing of the present application. No new matter has been added to the present application by reference to this known usage. Additionally, it is clear that the above-referenced text is consistent with the examples of metal organic or metalorganic materials and metal alkoxides provided in the original application, as set forth in the original text above.

As to the seventh instance of underlined text, it is clear from the list of materials following the term "metalloid," that use of that term is not new matter. Merely by way of example, the list includes a metalloid, silicon. U.S. Patent No. 5,973,177 is submitted herewith, merely by way of example, to demonstrate reference to silicon as a metalloid that predates the filing date of the present application.

In view of the foregoing, it is believed that the 35 U.S.C. 132 rejection of the Amendment of December 2, 2003 as to the above-mentioned replacement paragraph has been overcome. It is respectfully requested that this rejection and the cancellation requirement associated therewith be withdrawn.

Claims 37-44 were rejected under 35 U.S.C. Section 103(a) as allegedly being unpatentable over an article of Dulay *et al.*, *Preparation and Characterization of Monolithic Porous Capillary Columns Loaded with Chromatographic Particles*, Anal. Chem., Vol. 70, No. 23 (1998), 5103-5107 (hereinafter, "Dulay") in view of an article of Viklund *et al.*, *"Molded" Macroporous Poly(glycidyl methacrylate-co-trimethylolpropane trimethacrylate) Materials with Fine Controlled Porous Properties: Preparation of Monoliths Using*

Photoinitiated Polymerization, Chem. Mater., Vol. 9 (1997), 463-471 (hereinafter, "Viklund"). These rejections are moot in view of the cancellation of Claims 37-44.

It is submitted that new Claims 53-60 are patentable over Dulay in view of Viklund, as demonstrated in the remarks below and a Declaration of Maria T. Dulay that is submitted herewith. Dulay teaches a starting mixture of tetraethyl orthosilicate (TEOS), ethanol to solubilize the TEOS (which is not freely soluble in water), and a dilute HCl solution to acidify the mixture. (See Dulay, page 5104, and Declaration of Maria T. Dulay, paragraph 6.) The mixture undergoes a hydrolysis reaction, in which the ethanol does not participate, to form an inorganic $Si(OH)_4$ product and ethanol. (See Dulay, page 5104, and Declaration of Maria T. Dulay, paragraph 6.) By virtue of the amount of HCl and water in the mixture, the hydrolysis goes to completion, such that the TEOS is fully converted to the inorganic $Si(OH)_4$ product and ethanol. (See Declaration of Maria T. Dulay, paragraph 6.) Neither the inorganic $Si(OH)_4$ product nor the ethanol in the resulting mixture is a metal organic compound. (See Declaration of Maria T. Dulay, paragraph 6.)

As the resulting mixture has no chromatographic capability, Dulay must add a component that has such capability to produce a column with chromatographic capability. (See Declaration of Maria T. Dulay, paragraph 7.) Dulay teaches that various materials, namely, chromatographic octadecylsilica particles and bare silica, are added to the resulting mixture. (See Declaration of Maria T. Dulay, paragraph 7.) Dulay teaches that this resultant combination is sonicated and then introduced into capillary columns, whereupon a filled column is placed on a hot plate and heated above 373 K for about 24 hours. (See Dulay, page 5104, and Declaration of Maria T. Dulay, paragraph 8.) Under these conditions, the inorganic $Si(OH)_4$ in the column filling undergoes a condensation reaction in which the inorganic $Si(OH)_4$ polymerizes and the ethanol evaporates until the column is dry. (See Dulay, page 5104, and Declaration of Maria T. Dulay, paragraph 8.) This polymerization produces an inorganic porous matrix in which the chromatographic particles are embedded. (See Dulay, page 5104, and Declaration of Maria T. Dulay, paragraph 8.) The porous matrix itself comprises no metal organic polymer. (See Declaration of Maria T. Dulay, paragraph 8.)

As conceded by the Examiner in the now-moot rejections, Dulay does not teach irradiation of the filling in the column. (See also Declaration of Maria T. Dulay, paragraph 9.) It is submitted that Dulay also fails to suggest any such irradiation and additionally fails to teach or suggest a method that comprises a combination of elements as recited in Claim 53,

and Claims 54-60 depending therefrom. (See also Declaration of Maria T. Dulay, paragraph 9.)

In the now-moot rejections, the Examiner alleged that it would have been obvious to use photoinitiated polymerization in Dulay because of the alleged advantages disclosed in the abstract of Viklund, namely, ease of preparation, short time needed for reaction, and the possibility of running the reaction at low temperature. However, it is submitted that the alleged advantages mentioned in the abstract of Viklund would not have been read by one of ordinary skill as being relative to systems or methods disclosed in publications later than Viklund, such as Dulay. Further, as to ease, one of ordinary skill in the art would not have read Viklund's preparation as being of ease relative to Dulay's preparation, particularly in view of the fact that Viklund's preparation includes a preparation of the monomers (which takes overnight, or about 12 hours), an involved preparation of polymerization tubes (which takes over 8 hours), in addition to the preparation of the mixture used therein (which takes about 2 hours). (Viklund, pages 464-465.) As to time, Viklund's assertion of short reaction time is made relative to polymerizations that are allowed to proceed for 6 to 24 hours. (Viklund, page 465.) It is submitted that one of ordinary skill in the art would not have read Viklund's teaching as advantageous in terms of time, as Viklund's preparation includes an overnight preparation of monomers (about 12 hours), an involved preparation of polymerization tubes (over 8 hours), in addition to the preparation of the mixture used therein (about 2 hours), all of which takes over 22 hours. As to temperature, Viklund's assertion of the possibility of running the reaction at low temperature is made relative to the preparation of imprinted matrixes for molecular recognition. (Viklund, page 467.) It is submitted that one of ordinary skill in the art would not have read Viklund's teaching as advantageous as to all preparations. In view of the foregoing, it is submitted that one of ordinary skill in the art would not have been motivated to combine the disparate teachings of Dulay and Viklund as previously hypothesized by the Examiner. (See also, Declaration of Maria T. Dulay, paragraphs 11 and 12.)

Even if a combination of Dulay and Viklund were possible, *arguendo*, Viklund would not have made up for the failures of Dulay as to invention of Claims 53-60. Viklund teaches preparing an initial mixture that comprises benzoin methyl ether initiator, glycidyl methacrylate, trimethylolpropane trimethacrylate, isooctane and toluene; purging that mixture with helium; and transferring the resulting mixture to a pre-treated quartz tube, whereupon the tube is sealed and irradiated. (See Viklund, page 464-468, and Declaration of Maria T.

Dulay, paragraph 10.) The initial mixture does not comprise a metal alkoxide, the resultant mixture does not comprise a metal organic compound, and the ultimate monolith produced in the quartz tube does not comprise a metal organic polymer. (See Declaration of Maria T. Dulay, paragraph 10.) Thus, even if the alleged combination of Dulay and Viklund were permissible, *arguendo*, one of ordinary skill in the art would not have arrived at the invention of Claims 53-60. (See also, Declaration of Maria T. Dulay, paragraph 12.)

In view of the foregoing, it is submitted that one of ordinary skill in the art would have had no motivation, at the relevant time, to combine the disparate references of Dulay and Viklund in the manner previously hypothesized by the Examiner, and even if one so skilled would have been so motivated, *arguendo*, and such a combination were permissible, *arguendo*, one so skilled would not have arrived at the invention of Claims 53-60. It is respectfully submitted that Claims 53-60 define novel and non-obvious subject matter of the present invention, notwithstanding Dulay, Viklund, and any hypothetical combination thereof.

The Examiner indicates that of the substitute specification that Applicants submitted in clean form (Appendix I) and in marked form (Appendix II) on May 20, 2003, the Appendices are blanks and the marked form is apparently missing from the US PTO record. Applicants received a return receipt postcard that identified the Amendment and Appendices of May 20, 2003 and the total page count associated therewith and that bore a US PTO stamp dated May 22, 2003. Thus, it appears that these documents were received by the US PTO. Nonetheless, the Appendices are resubmitted herewith, with a reminder that since these Appendices were initially submitted on May 20, 2003, an Amendment was filed on December 2, 2003 and this Amendment is now being filed with amendments to the specification.

Conclusion

Claims 53-60 define novel and non-obvious subject matter of the present invention. Therefore, an early notification of allowability is earnestly solicited.

Respectfully submitted,

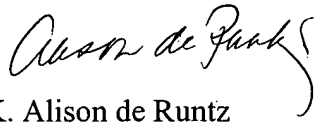

K. Alison de Runtz
Reg. No.: 37,119

PARSONS HSUE & DE RUNTZ LLP
655 Montgomery Street, Suite 1800
San Francisco, CA 94111
(415) 318-1160
(415) 693-0194 (Fax)

Metal-Organic Vapor Phase Epitaxy of III-V nitrides

J F. Carlin, C. Zellweger, J. Dorsaz and M. Ilegems

Our institute has acquired a metalorganic vapor phase epitaxy system for III-V nitride (In,Al,Ga)N materials. The ability to grow the main building blocks needed for GaN-based optoelectronics has been demonstrated by the fabrication of high performance blue LED devices.

A Metal Organic Vapor Phase Epitaxy (MOVPE) system AIX 200/4 RF-S, for the growth of III-V nitrides heterostructures for optoelectronics was installed in our institute and is operational since the beginning of year 2002. Sources for III-elements are TMGa, TMAl, TMIn and TEGa. NH_3 is used as active nitrogen source. Dopant sources are diluted SiH_4 for n-type and Cp_2Mg for p-type doping. Carrier gases are both nitrogen and hydrogen. The hydrogen is generated on-demand in a Hogen 40 system by electrolysis of de-ionized water; this avoids the stocking of H_2 and increases the system security. The susceptor can be heated by radio frequency power up to 1200°C. The system is equipped with a Luxtron 950 nm reflectivity measurement set-up that performs *in-situ* acquisition. This allows to precisely monitor the three phases of growth of GaN on sapphire wafers, i.e. the deposition of a low temperature nucleation layer, the recrystallization of this layer during ramping up of temperature and the onset of epitaxial growth at high temperature (see figure below). Growth rate is measured further by the frequency of the reflectivity oscillations.

The ability for the system to grow the necessary building blocks for GaN-based optoelectronic devices was demonstrated: smooth bulk GaN layers grown on sapphire, with high crystalline quality (< 300 arcsec FWHM on 0002 X-ray diffraction scans) and residual donor density below 10^{17} cm^{-3}; n-type (Si) and p-type (Mg) doping of GaN layers; high quality AlGaN alloy with Al content below 20%, demonstrated by the growth of AlGaN/GaN bidimensional electron gas structures with a mobility of 1000 $cm^2V^{-1}s^{-1}$ at 300K; and eventually, GaN/InGaN multi-quantum well showing efficient photoluminescence at 430 nm wavelength.

InGaN materials were also grown over the whole alloy composition range. The figure below illustrates one of the main difficulty to include both GaN and In-rich InGaN layers in the same epitaxial structure: that is that InGaN decomposes at low temperatures compared to GaN (see the inset, the reflectivity of InGaN samples suddenly rises when it decomposes to a metallic indium layer). The figure presents the InGaN decomposition temperature versus indium content. This limits the temperature at which further GaN layers can be grown; as high quality GaN is typically grown at 1000°C, we can see that special low-temperature growth conditions for (Al)GaN must be used after the deposition of InGaN with more than 20% In content.

Final benchmarking of the MOCVD system was done by the successful growth of a highly efficient InGaN/(Al)GaN light emitting diode (see next report).

Present research concentrates on the growth of distributed Bragg reflectors for physics and device application, and on the realization of multi quantum well structures with large conduction band offset for studies on intersubband transitions (collaboration with Neuchâtel University).

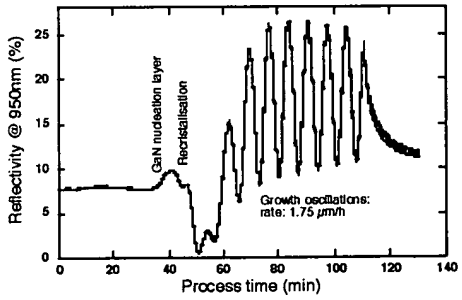

In-situ reflectance development during the growth of a standard GaN buffer layer on sapphire wafer

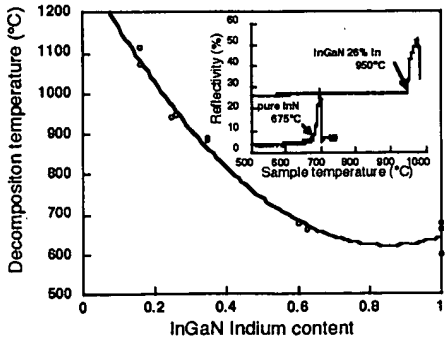

Temperature of decomposition of InGaN layers versus In content. Inset shows the measurement method, from in-situ reflectance signal during a ramp in temperature

EPITAXIAL LATERAL OVERGROWTH OF GaN WITH CHLORIDE-BASED GROWTH CHEMISTRIES IN BOTH HYDRIDE AND METALORGANIC VAPOR PHASE EPITAXY

R. Zhang[a,b], L. Zhang[a], D.M. Hansen[a], Marek P. Boleslawski[c], K.L. Chen[b], D.Q. Lu[b], B. Shen[b] Y.D. Zheng[b], and T.F. Kuech[a]

[a] Department of Chemical Engineering, University of Wisconsin, Madison, WI 53706
[b] Department of Physics, Nanjing University, Nanjing 210093, China.
[c]Aldrich Chemical, Milwaukee, WI

Cite this article as: MRS Internet J. Nitride Semicond. Res. 4S1, G4.7 (1999)

ABSTRACT

Epitaxial lateral overgrowth (ELO) of GaN on SiO_2-masked (0001) GaN substrates has been investigated by using chloride-based growth chemistries via hydride vapor phase epitaxy (HVPE) and metal organic vapor phase epitaxy (MOVPE). Diethyl gallium chloride, $(C_2H_5)_2GaCl$, was used in as the MOVPE Ga precursor. The lateral and vertical growth rates as well as the overgrowth morphology of ELO GaN structures are dependent on growth temperature, V/III ratio and the in-plane orientation of the mask opening. A high growth temperature and low V/III ratio increase the lateral growth rate and produce ELO structures with a planar surface to the GaN prisms. High-quality coalesced and planar ELO GaN has been fabricated by both growth chemistries. The use of the diethyl gallium chloride source allows for the benefits of HVPE growth to be realized within the MOVPE growth environment.

INTRODUCTION

GaN and related compounds are being developed for short wavelength light-emitting devices, such as laser (LD) and light-emitting diodes (LED), in addition to high temperature and high power electronics. GaN-based LEDs and LDs have been successfully developed and are being commercialized. Several factors impede the further development of GaN devices. A principal difficulty is the high density of dislocations within the GaN epilayers, which can be as high as 10^8-$10^{10}/cm^2$ [1]. Recently, epitaxial lateral overgrowth (ELO) has been demonstrated to effectively reduce the dislocation density in the GaN epilayers within the lateral overgrown regions [2]. Long-lifetime GaN LDs fabricated on ELO-grown materials has been reported [3]. Most reports on GaN ELO have used the metalorganic vapor phase epitaxy (MOVPE) growth technique [4,5]. Hydride vapor phase epitaxy (HVPE) is also a very attractive technique for GaN ELO. HVPE utilizes GaCl generated *in situ* through the reaction of liquid Ga with HCl. HVPE offers a high growth rate and high material quality for GaN growth [6,7]. The typical growth rate can be as high as 100-200 μm/hr. The halide process has been shown to offer a higher lateral-to-vertical growth rate ratio [8] than MOVPE materials, which is critical for ELO. GaN produced by the HVPE technique does result in a greatly reduced intensity of the defect-based luminescence referred to as the yellow band (YL) when compared to the TMG-based MOVPE materials. This has been attributed to the lack of carbon in the HVPE growth system but is present in the growth sources used in MOVPE-growth systems. Intentional carbon introduction

into HVPE materials can result in the appearance of YL [9]. If a controlled amount of GaCl can be introduced into a cold wall MOVPE reactor, a low carbon source could be combined with the advantages of the MOVPE reactor environment. Diethyl gallium chloride (DEGaCl) is used here as a Ga source in GaN ELO growth. DEGaCl will decompose to GaCl through the β-elimination reaction in the gas phase allowing the *in situ* formation of GaCl at relatively low gas phase temperatures:

$$(C_2H_5)_2GaCl \rightarrow GaCl + 2C_2H_4 + H_2 \qquad (1).$$

The decomposition of the DEGaCl to GaCl near the growth front makes it possible to realize a high quality growth of GaN through a HVPE chemistry at high V/III ratio. This source was successfully used in GaAs growth that resulted in high uniformity, low carbon content GaAs film [10, 11]. GaAs selective area growth, with a complete selectivity of GaAs growth with respect to SiO_2, Si_3N_4, and Al_2O_3 masking materials, has been demonstrated over a wide range of process window [12,13,14]. The present work demonstrates the utility of the DEGaCl source in GaN ELO. In this paper, we systematically investigate the GaN ELO by using both HVPE and MOVPE with DEGaCl as the Ga source. It has been found that both the growth rate and the geometric shape of the GaN prisms are dependent on the growth condition and the orientation of the window opening. High growth temperatures and a low V/III ratio are helpful in enhancing the lateral overgrowth. Under optimized growth conditions, high quality ELO GaN films are produced with a planar surfaces and free of observable voids at the coalescence interface.

EXPERIMENTS AND RESULTS

The initial GaN 'substrate' is a 1μm thick GaN film grown by MOVPE on a (0001) sapphire substrate. The masking material a ~100nm thick patterned CVD SiO_2 layer. There are two kinds of pattern used in this study. The first pattern is a radial pattern consisting of many ~5 μm wide stripe openings in the masking materials with a 0.74° angle separation. An additional pattern consisted of 2-4μm wide parallel stripe openings on a 12μm pitch oriented along the $<1\bar{1}00>$ orientation. The substrates were used in a subsequent ELO GaN growth step in both HVPE and MOVPE systems, with DEGaCl as the Ga source in the latter case. In the HVPE process, the growth temperature is varied over the range of 1030-1100°C. The input V/III ratio, calculated as the ratio of the input NH_3 to input HCl flow rates, is controlled between 33 to 83 corresponding to a NH_3 mole fraction, $[NH_3]$, of 0.076-0.12. Nitrogen was used as the carrier gas. In the MOVPE process, the growth temperature is varied over the range of 1000-1100°C, while the input V/III ratio is varied over the range of 1800-3400. The hydrogen is used as the carrier gas in this case.

The extent and properties of the GaN ELO on SiO_2-masked substrates were determined. Both the growth rate and the morphology of ELO regions depend on the growth conditions and stripe or opening orientation. Figure 1 presents the typical growth morphology, obtained through scanning electron microscopy (SEM) on a HVPE GaN ELO sample on a radial patterned substrate using the growth conditions of T_g=1050°C, input mole fraction $[NH_3]$=0.12 and HCl input mole fraction of [HCl]=0.0022. In the Figure 1(a) is an image of an ELO GaN prism obtained within an opening oriented along the $<11\bar{2}0>$ direction while Figure 1(c) is an image of a $<1\bar{1}00>$-oriented prism. The prism shown in Figure 1(b) was formed in a direction intermediate to the $<11\bar{2}0>$ and $<1\bar{1}00>$ directions. The prism cross-section changes with the

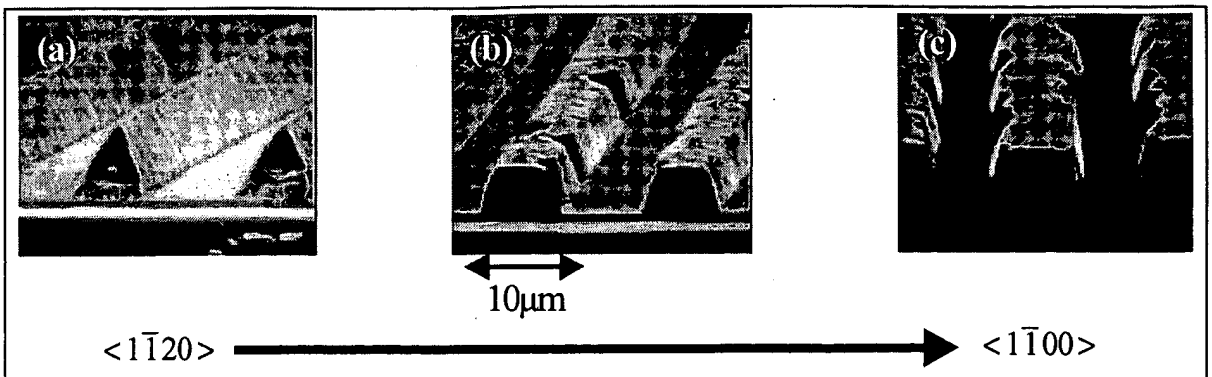

Figure 1: The orientation dependence of GaN ELO prisms grown by HVPE. The stripe opening was varied from the <11$\bar{2}$0> to <1$\bar{1}$00> in-plane directions.

different stripe orientations. The cross-section of the <11$\bar{2}$0> prisms is a triangle with a base angle of ~62°, which indicates that these prism sidewalls are (1$\bar{1}$01) planes. The cross-sectional shape of the<1$\bar{1}$00>-oriented prism is a trapezoid. It is worthwhile to point out that the <11$\bar{2}$0>-oriented prism has the smoothest sidewalls, while the <1$\bar{1}$00>-oriented prism has much rougher sidewalls. This may indicate that the (1$\bar{1}$01) planes are the more stable growth facets under these growth conditions. Both the lateral and vertical growth rates are dependent on the stripe opening orientation. From Figure 1, we find that the <11$\bar{2}$0>-oriented prism has the lowest lateral growth rate but the highest vertical growth rate. The <1$\bar{1}$00>-oriented prism has the highest lateral growth rate and the lowest vertical growth rate.

The SEM observations also reveal a strong dependence of the geometric prism shape on the specific growth conditions. Figure 2 shows two SEM micrographs of the cross-sections of GaN HVPE ELO prisms oriented along the <11$\bar{2}$0> and <1$\bar{1}$00> directions, respectively. The growth conditions employed for these samples were T_g=1100°C, [NH_3]=0.076 and [HCl]=0.023. The conversion efficiency of the HCl to GaCl is approximately 60-70%. As the growth temperature is elevated and the V/III ratio decreased, the cross-sectional shape of the ELO prisms change. The <11$\bar{2}$0> prism cross-section changes from a triangle to a rectangle, and that of the <1$\bar{1}$00> prism changes from a trapezoid to a reverse-trapezoidal structure. The latter result has not been previously reported in the GaN ELO literature.

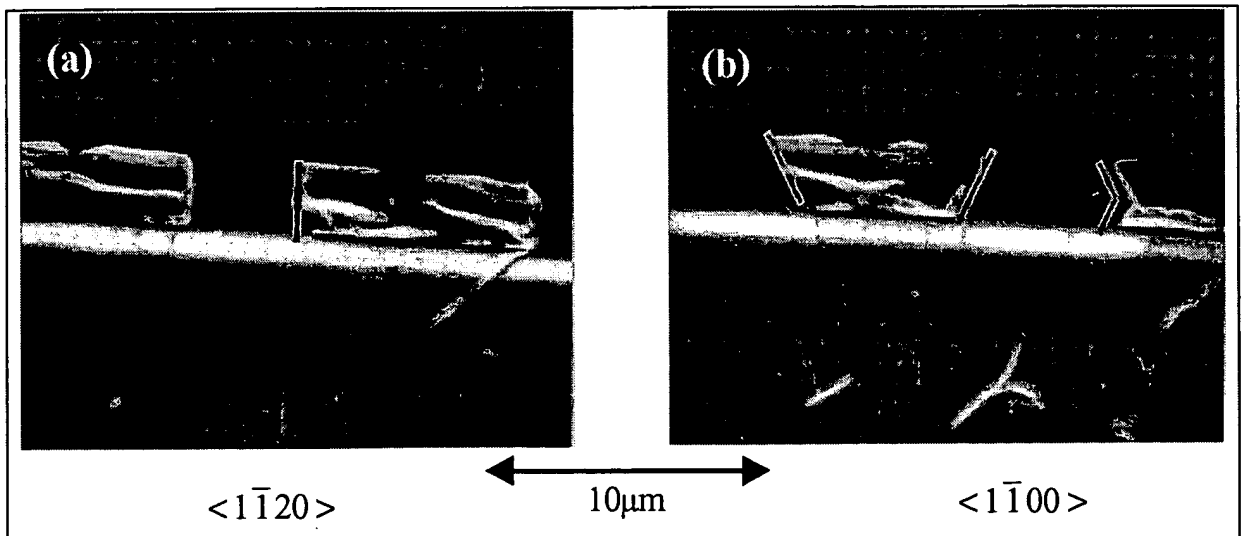

Figure 2: The orientation dependence of cross-sections of prisms grown under high temperature

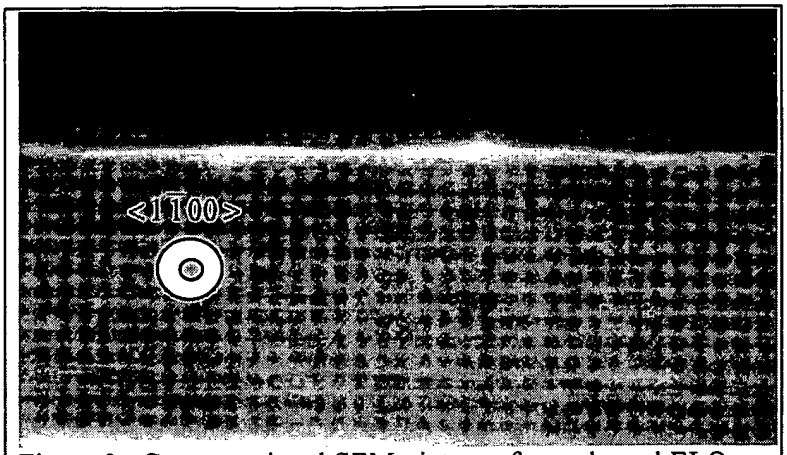

Figure 3: Cross-sectional SEM picture of a coalesced ELO GaN sample grown by HVPE. There is no void observed at the coalescence interface.

Under optimized growth conditions, high-quality coalesced ELO GaN films on parallel patterned substrates, having planar surfaces, have been fabricated by the HVPE technique. A cross-sectional SEM image of the coalesced film is shown in Figure 3. The growth temperature is 1100°C and $[NH_3]$=0.076, [HCl]=0.023 for this sample. No observable void was found at the coalescence interface under these conditions.

MOVPE GaN ELO, when using DEGaCl, exhibit similar trends to the HVPE samples. As shown in Figure 4, the MOVPE ELO GaN samples grown in $<1\bar{1}00>$-oriented parallel stripes under the same V/III ratio of 3500, have a changing morphology with growth temperature. The cross-section of ELO GaN prisms is strongly dependent on growth temperature over the range 1100°C to 1000°C. The cross-section of ELO GaN prisms grown at 1100°C is close to rectangular, while those of ELO GaN prisms grown at lower than 1050°C are triangular. The lateral growth rate of ELO GaN increases with increasing growth temperature while the growth temperature at this V/III ratio only weakly influences the vertical growth rate.

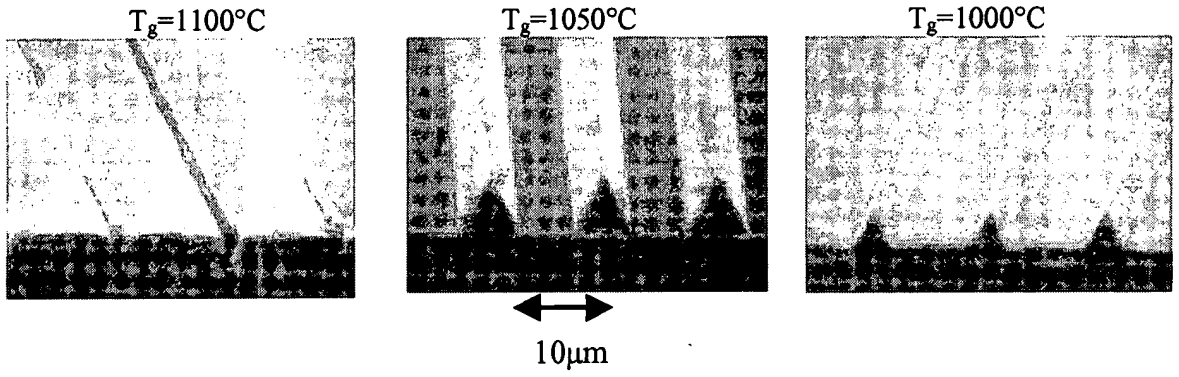

Figure 4: The growth temperature dependence of MOVPE ELO GaN by using DEGaCl on the $<1\bar{1}00>$- oriented parallel stripes with a constant V/III ratio of 3500.

The dependence of MOVPE GaN ELO, using DEGaCl, on the V/III ratio during growth has been investigated and is shown in Figure 5. These GaN ELO samples were grown at the growth temperature of 1100°C over the V/III ratio range of 3500-1800. The cross-section of ELO GaN prisms grown with V/III ratio of 1800 is rectangular, while those of ELO GaN prisms grown with higher V/III ratio are trapezoidal, with sloping facets becoming evident. The lateral and vertical growth rates are somewhat dependent on the V/III ratio at this temperature with a lower V/III ratio leading to a higher vertical growth rate.

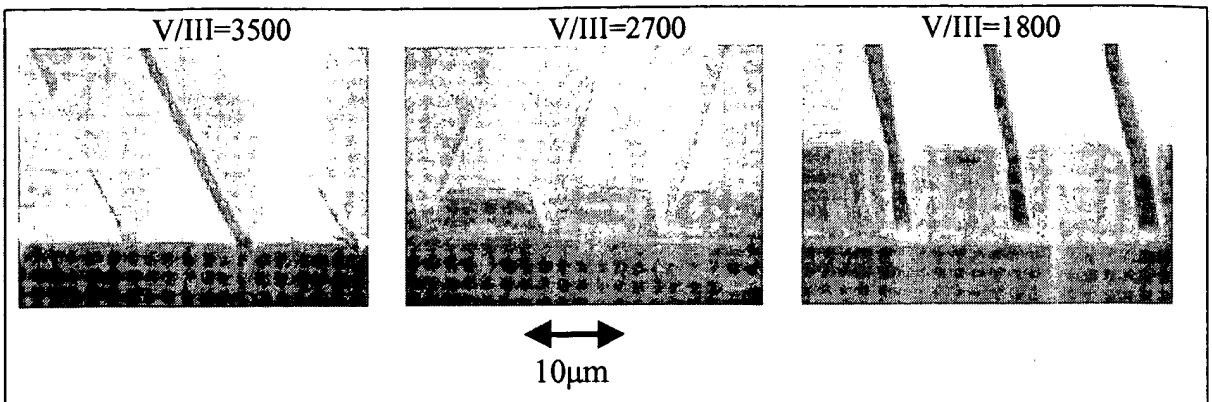

Figure 4: The dependence of MOVPE ELO GaN by using DEGaCl with the $<1\bar{1}00>$-oriented parallel stripes pattern at the constant growth temperature of 1100°C.

DISCUSSION

The resulting structure during the ELO process is known to be dependent on the gas phase transport of reactants to the growth front, which is dependent on the growth conditions and mask geometry. The difference in growth behavior between the inorganic, GaCl-based growth, and conventional MOVPE ELO using trimethyl gallium, also indicates that the growth chemistry plays an important role in the local growth rates and facet formation [8]. The chemical and physical properties of mask and substrate materials affect the surface diffusion [15], nucleation and kinetics. The lateral and vertical growth rates of ELO GaN are thus determined by the interplay of these various influences at the growth front. The local growth environments near a mask opening will differ from those in large-scale deposition and the optimization of the material properties and growth habit of the localized regions may be quite different from that found on non-masked regions. Under the conventional conditions for HVPE deposition, it has been suggested from the observed large surface roughness of HVPE-grown large scale GaN films that the (0001) plane is not the most stable growth facet [6]. Under such conditions, the most stable growth front is thought to be the $(1\bar{1}01)$ planes. Higher growth temperatures and lower V/III ratios decrease the supersaturation (driving force) [8]. The resulting lower growth rate would enhance the surface diffusion rate of reactants over the (0001) plane to adjacent, more favored growth facets and result in a higher lateral growth rate and a variety of prismatic structures. The use of a chloride-containing Ga source in both these systems allows for the addition of several chemical reactions to the growth front chemistry. The simplest set of chemical reactions important at the GaN growth front in the case of chloride-based growth is:

$$GaCl + NH_3 \rightarrow GaN + HCl + H_2 \qquad (2)$$

$$GaN + HCl \Leftrightarrow GaCl + \frac{1}{2}N_2 + \frac{1}{2}H_2 \qquad (3)$$

where in the DEGaCl case, the GaCl is generated through the intramolecular decomposition of the growth source as presented in Equation 1. Reaction 3 implies equilibrium between the steady state concentrations of HCl and GaCl at the growth front. The MOVPE growth front has often been considered to be near thermodynamic equilibrium [16]. If this is the case for the high temperature growth of GaN, the supersaturation at the growth front will decrease with increasing temperature due the reversible reaction associated with the HCl reacting at the GaN surface. A similarity between the growth habits and behavior between the HVPE and MOVPE-DEGaCl systems is therefore expected.

The presence of chlorine in the growth system can modify the growth habit from the trimethyl gallium based growth. Experimentally, the chloride-based systems lead to both higher lateral-to-vertical growth and desirable growth facets, such as vertical sidewalls over a broader range of growth conditions. The near surface concentration of GaCl in the HVPE system is

higher than in the DEGaCl systems. If adsorbed chlorine or GaCl species can stabilize certain facets, the higher concentration of GaCl within the HVPE would more readily promote the formation of specific facets, such as the $\{1\bar{1}00\}$ planes, over the DEGaCl-based MOVPE growth. Regardless of the specific chemical mechanism, the use of GaCl within either of these systems leads to improved ELO characteristics over conventional MOVPE growth using simple metal alkyls.

CONCLUSIONS

ELO of GaN has been systematically investigated by using chloride-based growth chemistry in both HVPE and MOVPE, through the use of DEGaCl, systems. The lateral and vertical growth rates as well as the morphology of the ELO regions depend on the growth condition and orientations of opening stripes. The high growth temperatures and a low V/III ratio enhance the lateral overgrowth. The reverse trapezoid prism has been fabricated in $[1\bar{1}00]$ stripes under the growth temperature of 1100°C and the V/III ratio of 33. Under the optimized ELO conditions, high quality flat-topped and coalesced GaN ELO films have been successfully fabricated and no observable voids found at the coalescence interface.

ACKNOWLEDGEMENTS

R. Z., K.L. Chen, D.Q. Lu, B. Shen and Y.D. Zheng thank the financial support of the China "863" national high-tech development program. The authors would like to acknowledge the financial support of the ONR MURI on Compliant Substrates, and the facilities support of the NSF Materials Research Science and Engineering Center on Nanostructured Materials and Interfaces, USA.

REFERENCES

1 F.A. Ponce and D.P. Bour, Nature, **386**, 351(1997).
2 A. Sakai, H. Sunakawa and A. Usui, Appl. Phys. Lett., **71**, 2259(1997).
3 S. Nakamura, M. Senoh, S. Nagahama, N. Iwase, T. Yamada, T. Matsushita, H. Kiyoku, Y. Sugimoto, T. Kozaki, H. Umemoto, M. Sano and K. Chocho, Appl. Phys. Lett., **72**, 211(1998).
4 O-H. Nam, M.D. Bremser, T.S. Zheleva and R.F. Davis, Appl. Phys. Lett., 71, 2638(1997)
5 H. Matsushima, M. Yamaguchi, K. Hiramatsu and Sawaki, Proc. 2nd Int. Conf. Nitride Semiconductors, Tokushima, Japan, 1997, p492.
6 N.R. Perkins, M.N. Horton, Z.Z. Bandic, T.C. McGill and T.F. Kuech, Mat. Res. Sci. Symp. Proc. **395**, 243 (1996).
7 R.J. Molnar, K.B. Nichols, P. Maki, E.R. Brown and I. Melngailis, Mater. Res. Soc. Symp. Proc., **378**, 479 (1995).
8 J-O Carlsson, Solid State & Mater. Sci., **16**, 161(1990).
9 R. Zhang and T.F. Kuech, Appl. Phys. Lett. 72, 1611-1613 (1997).
10 T. F. Kuech, R. Potemski and F. Cardone *J. Cryst. Growth* V124, 318-325 (1992).
11 A. Narmann, M.L.Yu *Surface Science* V270, 1041-1047 (1992).
12 T.F. Kuech, *J. Cryst. Growth* V115, 52-60 (1991).
13 Ko-ichi Yamaguchi, K. Okamoto, *Jpn. J. Appl. Phys.* V32 4885-4888, (1993).
14 Y. Shiraishi, N. Furuhata, A. Okamoto, *J. Cryst. Growth* V182, 255-265 (1997).
15 A. Usui and T. Nishinaga, Jpn. J. Appl. Phys., **36**, L899(1997).
16 G.B. Stringfellow, *Organometallic Vapor Phase Epitaxy,* (Academic Press, San Diego, 1989) Chap. 3.

M R S Internet Journal *of* Nitride Semiconductor Research

Volume 3, Article 20

Mg-enhanced lateral overgrowth of GaN on patterned GaN/sapphire substrate by selective Metal Organic Vapor Phase Epitaxy

B. Beaumont, M. Vaille, G. Nataf, A. Bouillé, J.-C. Guillaume, P. Vénnègues, S. Haffouz, Pierre Gibart
Centre de Recherche sur l'Hétéroépitaxie et ses Applications, CRHEA-CNRS

This article was received on Wednesday, July 22, 1998 and accepted on Thursday, September 10, 1998.

Abstract

Selective and lateral overgrowth by Metal Organics Vapour Phase Epitaxy (MOVPE) was carried out until coalescence to produce smooth and optically flat thick GaN layers. A GaN epitaxial layer is first grown using atmospheric pressure Metalorganic Vapour Phase Epitaxy on a {0001} Al_2O_3. substrate. Then a 30Å silicon nitride dielectric film is deposited in-situ by reaction of silane and ammonia to form a selective mask. Afterwards, the openings and the figures in the dielectric films are achieved using standard photolithographic technology. Stripes openings in the mask, revealing free GaN surface, are aligned in the <10 $\bar{1}$0> direction. Typical stripes spacing and width are 10 µm and 5 µm respectively. These patterned layers are further on used for epitaxial regrowth of GaN by MOVPE. The growth anisotropy and therefore the coalescence process is achieved by introducing $(MeCp)_2Mg$ in the vapour phase. A two-step process is reported which allows a dramatic reduction of threading dislocations density not only above the masked areas but also above the windows opened in the mask. With this process, very sharp bound exciton luminescence peaks are measured at low temperature in the overgrown GaN.

1. Introduction

Selective epitaxy has been widely developed for III-V semiconductors like GaAs, InP or Si [1]. More precisely, selective epitaxy allows an accurate control of the size and the shape of the overgrowth and therefore leads to the fabrication of quantum structures (quantum wire and quantum dots). Selective epitaxy in heteroepitaxial systems like GaAs/Si [2] or InP/Si [3] has also been widely used to overcome the deleterious effect of the large lattice mismatch.

Selective epitaxy of GaN by both MOVPE and HVPE on patterned GaN on sapphire has been previously reported [4] [5] [6] [7] [8] [9] [10] [11] [12] [13] [14] [15]. Selective epitaxy corresponds to spatially controlled growth of an epitaxial layer through openings in a masking material, which is typically a dielectric such as silicon oxide or nitride. Growth anisotropy corresponds to the occurrence of different growth velocities on different crystallographic planes. This has been observed in HVPE since at least two decades ago. For instance in GaAs there are two orders of magnitude difference between the growth rates of $\{111\}_{Ga}$ and $\{1\bar{1}1\}_{As}$. These features are understood by analyzing the orientation dependence of the growth rate associated with surface kinetics. Growth anisotropy in MOVPE occurs

only when diffusing molecules encounter different surface orientation within their mean free path λ_s.

A major problem in selective epitaxy is the ability to provide real selectivity, with growth occurring only in the openings and without any deposits formed on the mask. This can be achieved when the supersaturation of the growth nutrients on the dielectric mask is sufficiently low to prevent any deposition whilst the nucleation barrier on the exposed substrate in the openings is low in comparison. Therefore, in VPE (MOVPE or HVPE), the non-occurrence of growth on the mask depends on the reaction parameters: temperature, pressure and mole fraction of active species.

2. Growth experiments

The growth of GaN is performed in a home-made MOVPE vertical reactor operating at atmospheric pressure. The carrier gas is either pure N_2 or a mixture of N_2:H_2. NH_3 and the different organometallic species (TMGa, $(MeCp)_2Mg$) and diluted silane are introduced into the growth chamber by dedicated lines. A rotating susceptor holds one inch diameter sapphire substrates with (0001) orientation. This reactor is equipped with a HeNe laser reflectometry set-up used to monitor in-situ the growth process, providing a real time insight on the growth rates and the surface smoothness of the growing samples. In the case of GaN regrowth on patterned GaN layers, it has been used to assess the completeness of the coalescence.

2.1. Preparation of the masked GaN templates

Patterned substrates used in this work are sketched on figure 1. After deposition of the GaN buffer layer at 600°C, a 2-3 μm thick GaN layer is grown at 1080°C on a one inch substrate. Detailed description of this growth process is given in [16]. The growth rate is about 2.8 μm/h. X-Ray rocking curves are typically 4 arcmin large. The threading dislocations density determined by TEM observation is in the 10^8 defects/cm^2 range.

The dielectric film was silicon nitride deposited on the GaN MOVPE layer. To this end, after completion of the growth of GaN, diluted silane is introduced in the vapor phase together with NH_3, allowing the *in situ* deposition of a thin (3 nm) layer. The silicon nitride was patterned using standard photolithography technology, revealing the free surface of the underlying GaN. For the realization of GaN pseudo-substrates, a 10 μm period grating with 5 μm wide stripes aligned along $[10\bar{1}0]_{GaN}$ covering the whole area of the 1" substrate was used. Figure 2 shows the HRTEM image cross section of such a patterned substrate on which GaN was overgrown. The scale is given by the inter-reticular distance in GaN (2.5Å between horizontal planes). The silicon nitride film is amorphous.

The selectivity of the growth is obtained with a high H_2 partial pressure (0.3 atm) in the growth chamber. When pure N_2 is used as carrier, a high density of nuclei is observed. Figure 3 shows the aspect of GaN regrowth on a mask containing stripes scanning all the crystallographic directions by 5° increment and an array of circular holes. This figure shows clearly that no parasitic nucleation occurs on the silicon nitride mask nearby the openings.

2.2. GaN regrowth

GaN regrowth conditions used in this work are exactly the same as those used for epitaxy on non masked substrates. The growth temperature is 1080°C. The total flow is 6 sl/mn with partial pressures of NH_3 and TMGa respectively of 0.3 and 10^{-4} atm. The regrowth is performed at atmospheric pressure.

The shape of undoped GaN ribs after a few minutes of growth on patterned substrates is schematically drawn on figure 4. The GaN stripes present a trapezoidal cross section with a top C facet and two slants oriented on the average along {11-22}. These slants are themselves facetted by {10-11} plane segments due to the high instability of the {11-22} growth plane. The slants form an angle θ of 58° with the basal C plane.

A schematic cross section of the GaN stripes for longer growth time is shown in figure 5. Dashed lines indicate different intermediate stages of the development of these stripes. During the growth, the two edges of the top C facet are moving along linear trajectories (provided constant growth rates) indicated by arrows. Note that if the angle θ is determined only by the structural properties of GaN, the angle α depends also on the anisotropy of the growth i.e. the ratio of vertical to lateral growth rates. A kinematic model involving only the delimiting planes mentioned above yields the following expressions for the coordinates (x, z) of the points A, B and C defined on figure 5:

$$\text{Point A: } (1/2\ W_O\ ,\ 0) \tag{1}$$

$$\text{Point B: } (1/2\ W_O + (G_S - G_C \cos(\theta))\ t / \sin(\theta)\ ,\ G_C\ t) \tag{2}$$

$$\text{Point C: } (1/2\ W_O + G_S\ t / \sin(\theta)\ ,\ 0) \tag{3}$$

where W_O is the width of the stripe opening in the mask, G_C and G_S are the growth rates in directions normal to the C facet and the slant respectively and t the growth time. The growth rates are assumed to be constant and the linear dependence on time holds as a first order approximation. The points A', B' and C' are obtained by simple symmetry. From Equation 1 and Equation 3, α is derived as:

$$\mathrm{tg}(\alpha) = \sin(\theta) / (\cos(\theta) - G_S/G_C)\ . \tag{4}$$

A straightforward interpretation of Equation 4 is that if G_S/G_C is lower than $\cos(\theta)$ then α is less than 90° and the two trajectories issued from A and A' are converging. As observed experimentally, this is the case for the regrowth of undoped GaN with the growth conditions stated above. This anisotropy is unfavorable for planarization during coalescence because the top C facet vanishes at the crossing of the two trajectories and the surface of the regrowth is constituted by slants only. An example of such behavior is given in figure 6 showing the cross section of a sample obtained with low growth rate but a long growth time. At this scale the silicon nitride mask cannot be seen. The voids at the coalescence boundary generally reported are not observed too. This is due to the small growth rate for this particular sample.

2.3. Regrowth of GaN with Mg doping

Particular growth conditions must be used to achieve favorable anisotropy of the growth i.e. stable C facets and vanishing slants in order to obtain smooth and planar surface after coalescence is completed. Up to now, the growth temperature was the only parameter reported in the literature that can be adjusted to obtain flat coalesced samples [17]. The cross section of the GaN overgrown stripes tend to be delimited with increasing temperature by vertical sides and a stable C top facet. In a previous work, we reported that the anisotropy of GaN in standard growth conditions is dramatically modified by magnesium doping [18]. The main effect of Mg doping is to reduce to the growth rate G_C in [1] direction without substantially modifying the growth rate G_S of the slants. But the cross section of the GaN:Mg stripes is still delimited by facets having the same crystallographic orientation than in the

undoped case.

Therefore, keeping standard growth conditions, the anisotropy G_S/G_C can be adjusted by introducing a sufficient amount of Mg precursor in the vapor phase so that the slants become the fast planes and vanish during coalescence. Figure 7 shows the cross section of a sample obtained by lateral overgrowth of Mg-doped GaN on patterned GaN substrates (5 μm opening with 10 μm period). By contrast to figure 6, the surface of the overlayer is smooth and we observe clearly voids buried at the foot of coalescence boundaries. The planarization was completed after about 2 hours growth run. Figure 8 illustrate diagrammatically how the shape of the stripes is evolving in the Mg doped overgrowth case. G_S/G_C is now greater than $\cos(\theta)$, α is more than 90° and the geometrical result is that the trajectories of the top facet edges diverge correspondingly. An expansion of the C facet is obtained.

2.4. A two-step lateral overgrowth process

Samples, as shown in figure 7, covering one inch diameter patterned GaN/sapphire substrate meet the flatness requirement for pseudo GaN substrates to be used further for the growth of devices structures. But the most important feature expected from the lateral overgrowth process is a large reduction of the density of threading dislocations which are mainly responsible for the short life time of high current injection devices or for the low mobility of undoped GaN. The target is to obtain GaN layers free of threading defects within areas compatible with devices geometry. In GaN, it is known that most of the threading defects are due to low angle boundaries existing within the mosaic structure of the epilayers. Moreover these defects thread in the growth direction along the C axis and their density is not reduced substantially when increasing the thickness of the sample.

On one hand, we observed [14] by HRTEM on cross sections of GaN samples grown on patterned substrates with anisotropy unfavorable to planarization (i.e. no doping with standard growth conditions) that (i) the defect lines above the masked area lie parallel to the basal plane (0001), (ii) the 90° line bending is initiated above the windows in the mask. This was also mentioned in the literature [19] where the bending points of the defect lines are reported to be contained in the trace of the {10-11} slants. On the other hand, when the growth anisotropy is favorable for the planarization (high growth temperature or with Mg doping in our work), the overgrown GaN is reported to be free of emerging defects above the masked areas but the threading defects originated from the underlying GaN still propagate vertically through the mask opening and then emerge at the top surface of the overgrowth.

Following these experimental facts, we have investigated a two-step process for the lateral overgrowth of GaN. In the first step, undoped GaN is overgrown until the top C facets vanish. In the second step, Mg is introduced to produce the coalescence with planarization. The first step is intended to initiate defects lines bending over the openings of the mask whereas the second step aims to planarization. This two step process is schematically shown on figure 9.

Figure 10 shows the SEM view of the cross section of a sample grown following this two steps process. No metallization was applied in order to resolve the resistivity contrast between undoped and Mg doped GaN. The growth run has been stopped before completeness of the planarization. During step (1), a surface having a "saw tooth" section is achieved with peaks and valleys. As soon as the Mg dopant is introduced, as discussed above, the slowly growing C top facets reappear. Due both to the deep and sharp V-shaped valley created during (1) and to the sudden change in the growth anisotropy in (2), limited diffusion of the nutrients results in the creation of voids in the valleys [1]. This phenomenon can be avoided by stopping step (1) before two neighboring stripes come in contact. Then the valley is rather U-shaped, with wide angles formed between the two slants and the mask as sketched in figure 5. On figure 10, t_1 and t_2 represent the lateral expansion of the slants without and with Mg doping respectively. They are found to be proportional to the growth time allowed for each step and this tends to prove that Mg affects only the growth on C plane whereas the growth rate of the slant is not notably

modified (G_S ~0.7 μm/h for this sample). t_3 is the expansion of the C top facet after its reappearance, t_2/t_3 gives an estimate of 3.2 for the growth rates ratio G_S/G_C. The average measurements of α give for G_S/G_C a value of about 3 in good agreement with the previous one.

Finally figure 11 is the SEM tilted view of a sample on GaN overgrown with the two step process with complete planarization and terminated by an undoped GaN layer. Very smooth surfaces are obtained. The arrow points to an hexagonal pit formed at the coalescence boundary. Along the cross section a periodic grating of voids is seen. This sample is about 16 μm thick.

3. Assessment of the two-step GaN overgrowth.

3.1. Mg incorporation

Figure 12 is the SEM cross section of two-step GaN overgrowth on GaN masked layer observed at low temperature (100K) without metallization. The structure of the sample consists in a masked GaN layer grown in a first run on sapphire, the two-step GaN and finally an undoped GaN are deposited on top in a second run. For some samples, the undoped top layer has been deposited during a third run after cleaning the reactor in order to limit the contamination by Mg due to a memory effect.

Dashed vertical white lines are the coalescence boundaries separated by a 10 μm period. Plain white lines localize the border between steps 1 and 2. At low temperature, the volume filled during step 2 appears to be inhomogeneous. It is constituted by two zones delimited by a zigzag line along which the two dashed arrows are drawn. These volumes are labeled 2^S and 2^T. Volume 2^S is filled during lateral overgrowth by expansion of the slants whereas 2^T during expansion of the top C facets. The apparent inhomogeneity is confirmed by cathodoluminescence study of the cross section. The three spectra plotted in the inset are measured in the cross section of volumes 1, 2^T and 2^S. Volume 1 has a typical spectrum with bandedge emission of undoped GaN. Spectra of the volumes 2^S and 2^T correspond to GaN with low and high concentration of Mg dominated respectively by donor-acceptor pairs recombination and the deep blue luminescence band [20]. We have checked by cathodo-luminescence mapping that Mg doped GaN grown during step 2 is divided in two regions only. Above the zigzag line, the white gray zone is uniformly highly Mg doped GaN whereas below that line the darker gray zone corresponds to uniformly lightly Mg doped GaN. Most probably the zigzag line is a visualization of the trajectory of the C facets edges during the regrowth as the kinematic model predicts.

The origin of the inhomogeneous Mg distribution may be due to an anisotropy of its incorporation on different crystalline growth planes. But the difference in doping level may also be related to the observed difference in growth rates. The informations given by luminescence are only qualitative and SIMS analysis will be performed to check if the Mg atomic concentration in volume 2^S and 2^T are inversely proportional to their growth rates.

3.2. Observation of the threading defects bending

Figure 13 is the cross section TEM image of a two-step GaN overgrown on a patterned substrate. Threading dislocations present in the underlying masked GaN propagate vertically in the overgrown GaN through the mask opening. But all of them bend by 90° at points indicated by short arrows. During subsequent growth, the bent defect lines merge into the coalescence boundary. It is noticed that these points tend to organize along two lines visualized on the figure by the converging long arrows. A clear planar symmetry exists in this bending phenomenon. This reflects the symmetrical growth on both side of a plane parallel to and equidistant from the coalescence boundaries delimiting the periodic stripe patterns. The lines drawn through the bending points are likely to be the trajectory of the edges of the

vanishing top C facets. This suggests that bending occurs when a threading dislocation line crosses the right or left moving edge of the top C facet. As a result, when the top C facet has fully vanished at the end of step 1 of the process, all threading lines have been crossed and bent by 90° either to left or to right depending on their relative position from the middle of the mask opening. Therefore after that time, during step 2, the whole upper volume of the overgrowth comprised between the coalescence boundaries is free of vertically threading defects as observed by TEM observation on plane views.

Though the exact mechanism responsible for the bending is not known yet, a tentative view of this two-step process could be as schematically drawn on figure 14. At the end of step 1, during which the lateral growth is negligible, the slant is constituted by the cross section of the misoriented columns arising from the GaN masked layer. During step 2, the growth is mainly lateral and the columnar mosaic [21] is replaced by a lamellar stacking with low angle misorientations being accommodated in the basal plane.

3.3. Luminescence of GaN by epitaxial lateral overgrowth

Figure 15 shows the luminescence spectrum of undoped GaN grown on top of a pseudo-substrate obtained by the two-step process described above after reactor cleaning to minimize Mg contamination. This kind of spectrum is representative and has been observed with small variation for different samples grown following the same process. The main feature is the sharpness of the peaks. GaN layers grown directly on sapphire in the same reactor have FWHM of about 3 meV in the best cases. FWHMs below 1 meV are achieved for bound excitons. This is comparable to results reported for homoepitaxial GaN [22] and HVPE GaN [23]. The free excitons A and B are well resolved as well as the three emission lines labeled A* attributed to excited states of A following [23].

4. Conclusion

We have developed a two-step growth process to obtain pseudo GaN substrates by epitaxial lateral overgrowth on patterned GaN deposited on sapphire. In the first step, the vertical threading defects are bent by 90° during the shrinking of the top C facet delimiting the GaN ribs. In the second step, owing to the effect of Mg doping on the growth anisotropy, planarization of the surface is achieved during coalescence. This two-step process results in a reduced defect density over the masked area but also over the openings in the masked. The area available for growth of devices structures is then comprised between the coalescence boundaries in which the emerging defects are confined. It is shown that the luminescence of GaN is strongly improved as far as intensity and sharpness of the emission lines are concerned.

Acknowledgments

The authors would like to thank M. Passerel, M. Leroux, M. Teisseire and G. Neu for their helpful contribution to this work. Special thanks are also expressed to Y. Genuist from LSP-CNRS for cathodoluminescence experiments. This work is supported by an EU contract ESPRIT LTR-LAQUANI 20968.

References

[1] L. Jastrzebski, *J. Cryst. Growth* ***63***, 493 (1983).

[2] D. Pribat, B. Gerard, M. Dupuy, P. Legagneux, *Appl. Phys. Lett.* ***60***, 2144 (1992).

[3] O. Parillaud, E. Gil-Lafon, B. Gérard, P. Etienne, D. Pribat, *Appl. Phys. Lett.* ***68***, 2654 (1996).

[4] Y. Kato, S. Kitamura, K. Hiramatsu, N. Sawaki, *J. Cryst. Growth* ***144***, 133 (1994).

[5] S. Kitamura, K. Hiramatsu, N. Sawaki, *Jpn. J. Appl. Phys.* ***24***, L1184 (1995).

[6] T Detchprohm, T Kuroda, K Hiramatsu, N Sawaki, H Goto, *Inst. Phys. Conf. Ser.* ***142***, 859-862 (1996).

[7] D. Kapolnek, S. Keller, R. Vetury, R.D. Underwood, P. Kozodoy, S.P. DenBaars, U.K. Mishra, *Appl. Phys. Lett.* ***71***, 1204-1206 (1997).

[8] O-H Nam, MD Bremser, TS Zheleva, RF Davis, *Appl. Phys. Lett.* ***71***, 2638-2340 (1997).

[9] Tsvetanka S. Zheleva, Ok-Hyun Nam, Micheal D. Bremser, Robert F. Davis, *Appl. Phys. Lett.* ***71***, 2472-2474 (1997).

[10] O Nam, MD Bremser, BL Ward, RJ Nemanich, RF Davis, *Jpn. J. Appl. Phys.* ***36***, L532 (1997).

[11] A Usui, H Sunakawa, A Sakai, AA Yamaguchi, *Jpn. J. Appl. Phys.* ***36***, L899 (1997).

[12] Hugues Marchand , J.P. Ibbetson, Paul T. Fini , Peter Kozodoy , S. Keller, Steven DenBaars , J. S. Speck, U. K. Mishra, *MRS Internet J. Nitride Semicond. Res.* ***3***, 3 (1998).

[13] Zhonghai Yu , M.A.L. Johnson, T. Mcnulty, J.D. Brown, J.W. Cook,Jr, J.F. Schetzina, *MRS Internet J. Nitride Semicond. Res.* ***3***, 6 (1998).

[14] B. Beaumont, P. Gibart, M. Vaille, S. Haffouz, G. Nataf, A. Bouillé, *J. Cryst. Growth* ***189/190***, 97 (1998).

[15] S Nakamura, M Senoh, S Nagahama, N Iwasa, T Yamada, T Matsushita, H Kiyoku, Y Sugimoto, T Kozaki, H Umemoto, M Sano, K Chocho, *Appl. Phys. Lett.* ***72***, 211-213 (1998).

[16] P. Vennegues, B. Beaumont, S. Haffouz, M. Vaille, P. Gibart, *J. Cryst. Growth* ***187***, 167 (1998).

[17] O-H Nam, T. S. Zheleva, MD Bremser, RF Davis, *J. Electron. Mater.* ***27***, 233 (1998).

[18] B. Beaumont, S; Haffouz, P. Gibart, *Appl. Phys. Lett.* ***72***, 921 (1998).

[19] A Sakai, H Sunakawa, A Usui, *Appl. Phys. Lett.* ***71***, 2259-2261 (1997).

[20] M. Leroux, B. Beaumont, N. Grandjean, P. Lorenzini, S. Haffouz, P. Vennegues, J. Massies, P. Gibart, *Mater. Sci. Eng. B* ***50***, 97 (1997).

[21] F. A. Ponce, *MRS Bull.* ***22***, 51-57 (1997).

[22] H. Teisseyre, G. Nowak, M. Leszczynski, I. Grzegory, M. Bockowski, S. Krukowski, S. Porowski, M. Mayer, A. Pelzmann, Markus Kamp , K. J. Ebeling, G. Karczewski, *MRS Internet J. Nitride Semicond. Res.* ***1***, 13 (1996).

[23] A. Hoffmann, L. Eckey, *Mater. Sci. Forum* ***264/268***, 1259 (1998).

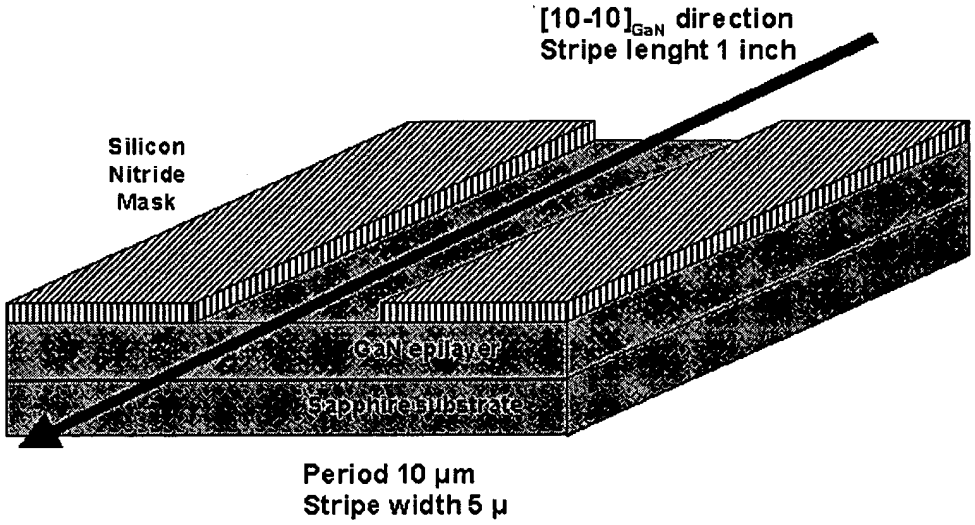

Figure 1. Structure of the patterned GaN on sapphire template typically used to study epitaxial lateral overgrowth of GaN. A 30 Å amorphous silicon nitride film is formed in situ immediately after growing the GaN epilayer. Windows in the mask are opened by reactive ion etching.

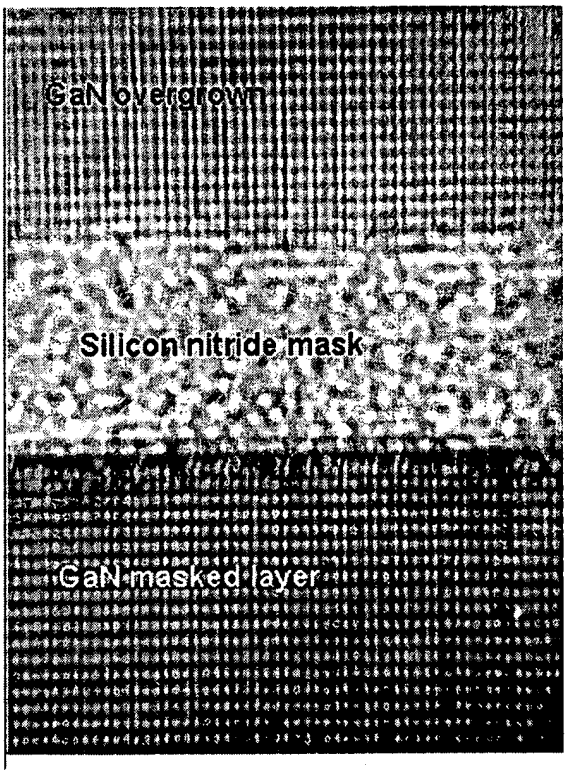

Figure 2. HR-TEM view of a cross section of the GaN overgrown on a masked and patterned GaN layer. The silicon nitride mask is about 30 Å thick.

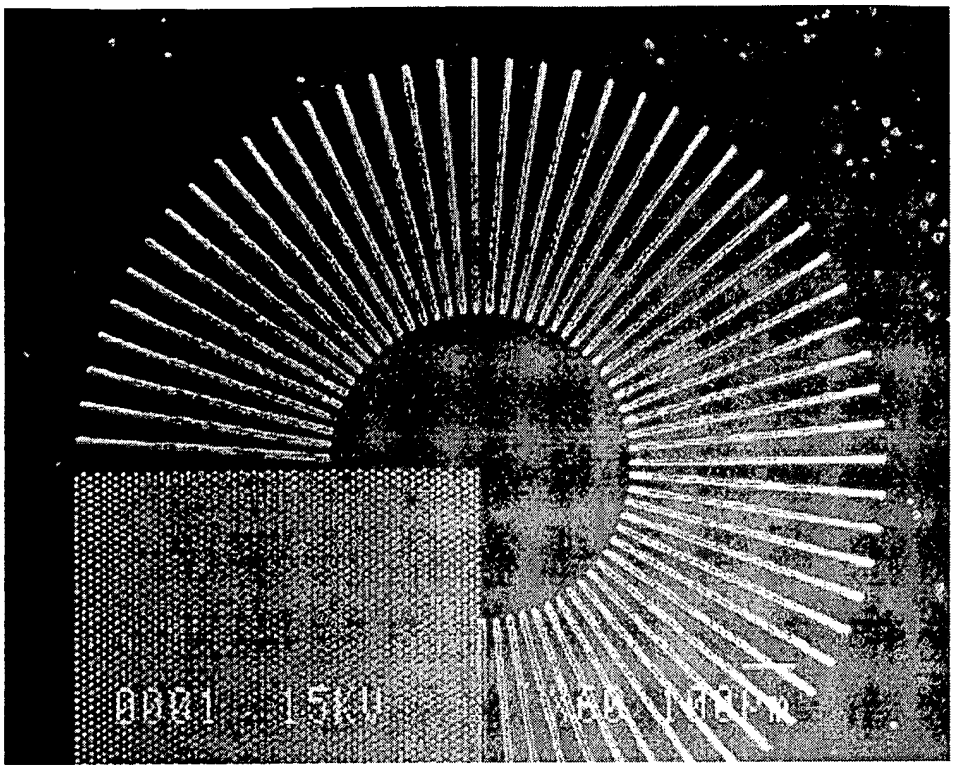

Figure 3. SEM top view of a star pattern mask. No parasitic nuclation is observed in the inner masked area whose diameter is 650 μm nor between the stripes. The marker is 100 μm.

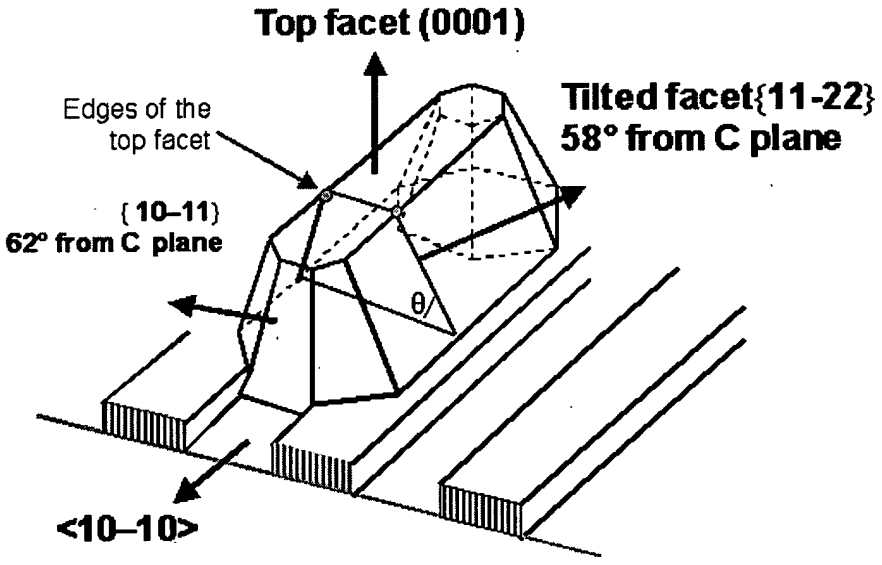

Figure 4. Schematic view of the GaN stripes at the beginning of the regrowth on the patterned substrates of figure 1.

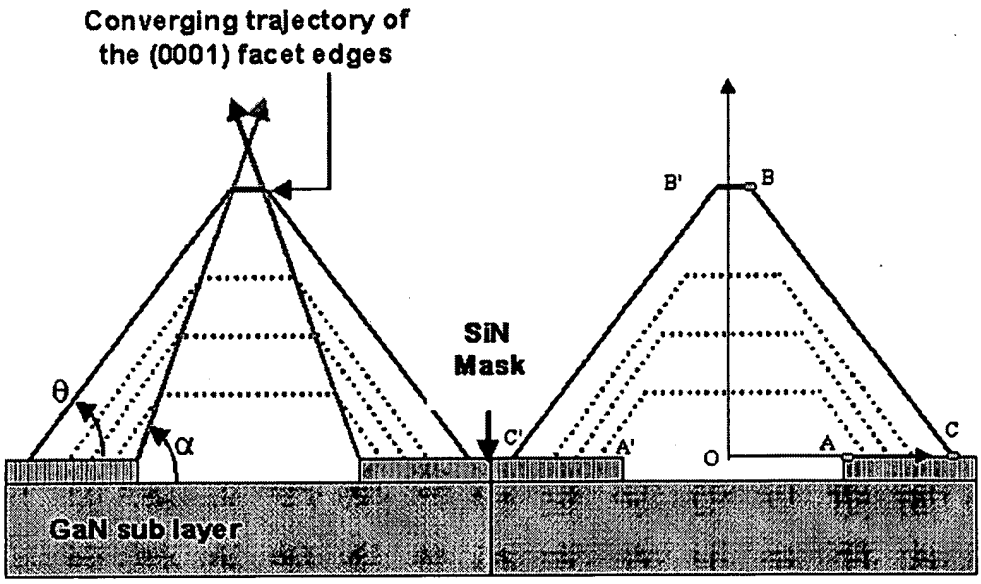

Figure 5. Schematic cross section of the GaN stripes for longer growth time. Dashed lines are different intermediate stages of the development of these stripes. During the growth, the two edges of the top C facet are moving along linear trajectories (provided constant growth rates) indicated by arrows. For undoped GaN, the top C facet vanishes above the crossing of the two trajectories. Note that if θ depends only on the structural properties of GaN, α is determined by the anisotropy of the growth i.e. the ratio of vertical to lateral growth rates.

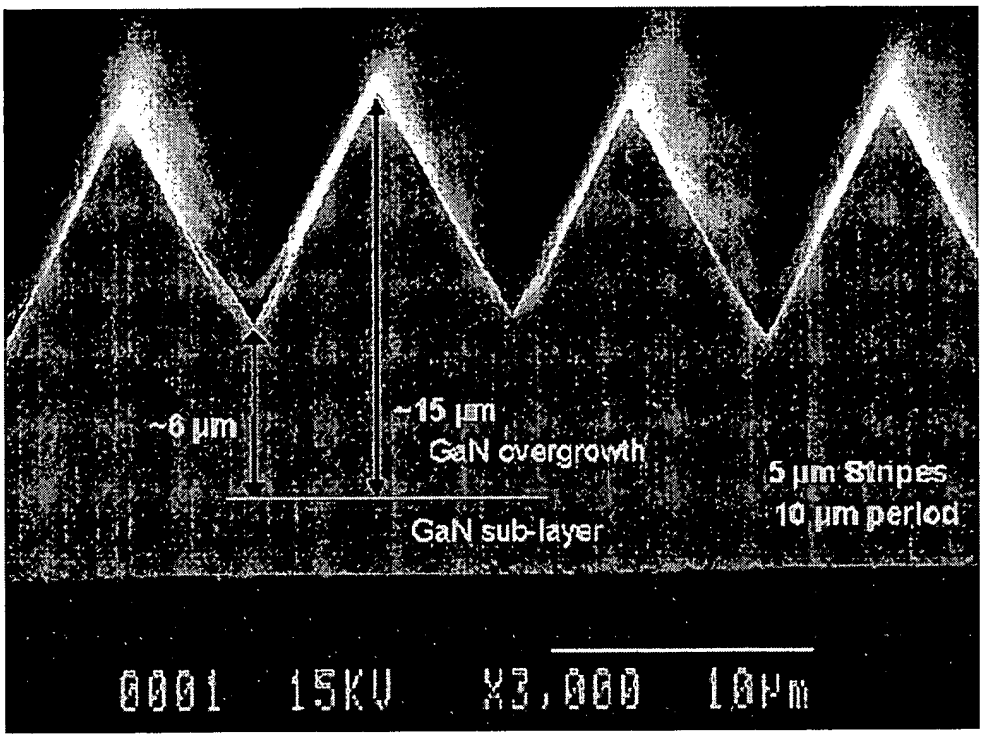

Figure 6. SEM cross section of lateral overgrowth of undoped GaN in standard conditions. Though perfect coalescence is obtained (without voids at the coalescence boundaries due to very slow growth rates), no smoothing is achieved.

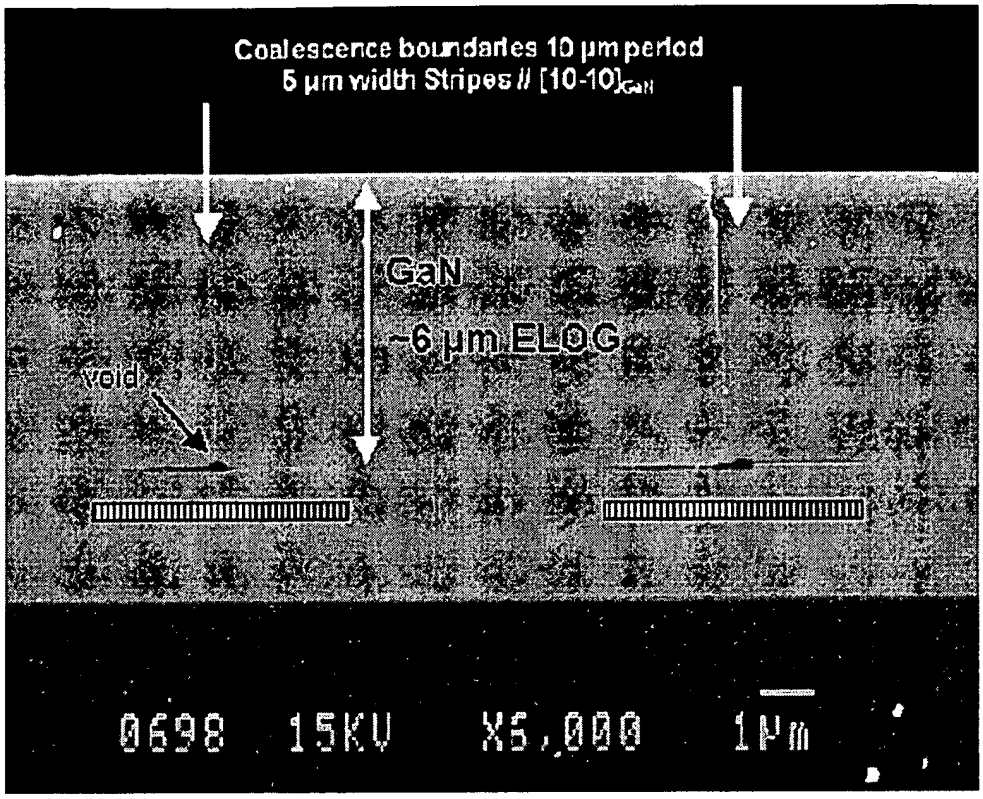

Figure 7. SEM cross section on Mg doped GaN overgrown at 1080°C on patterned substrate. Flat surface, contrasting with figure 6, is obtained due to the favorable growth anisotropy induced by the Mg doping. The mask appears as a very thin line above the dashed filled rectangle.

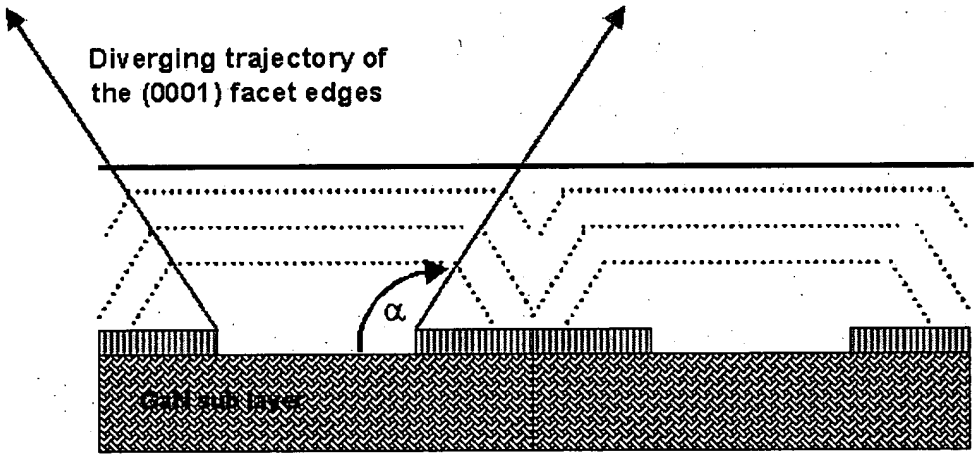

Figure 8. Schematic cross section of the Mg doped GaN. During the growth, the two edges of the top C facet still move along linear trajectories but due to doping, these trajectories are now diverging and the two slants are vanishing during coalescence as shown by the intermediate shapes (dashed lines).

Figure 9. Schematic principle of the two step GaN lateral overgrowth process. In step (1), undoped GaN is grown at 1080°C. In these conditions, the top C facets vanish. In step (2), under the same growth conditions but due to Mg doping, the C facets become the slow planes therefore reappearing and leading to planarization by expansion. The

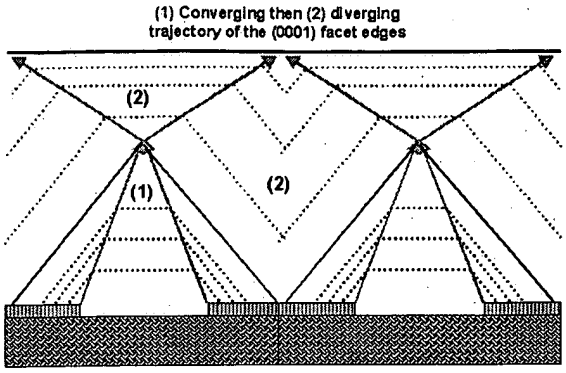

arrows represent the trajectories of the C facet edges.

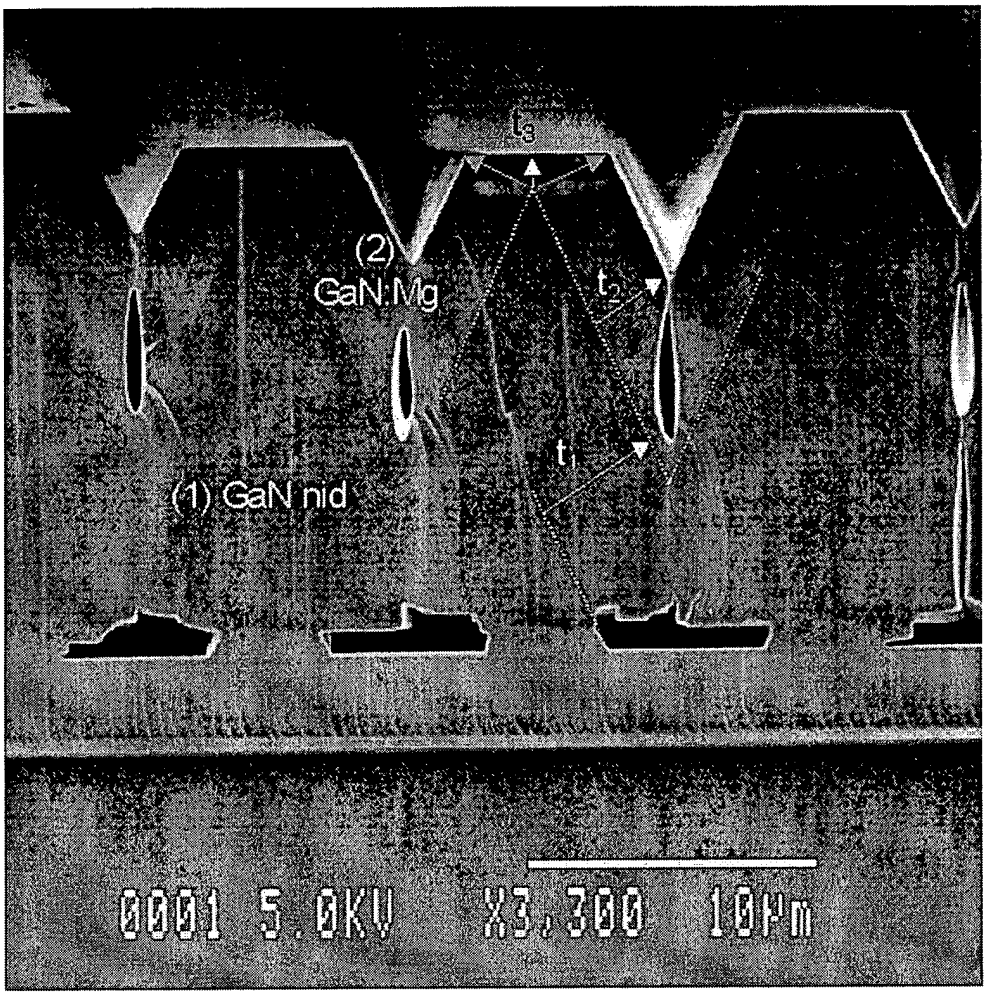

Figure 10. SEM cross section view of lateral overgrown GaN following the two step process. The sample was not metallized in order to observe resistivity contrast between (1) undoped (dark gray) and (2) Mg doped (light gray) GaN. In (1) a peaky surface as in figure 6 is obtained, the dashed line was drawn as a guide for the eye. In (2) the top C facets have reappeared and expand following the arrows. Note that voids are created in the deep valley of (1) during (2) mainly due to diffusion limited growth.

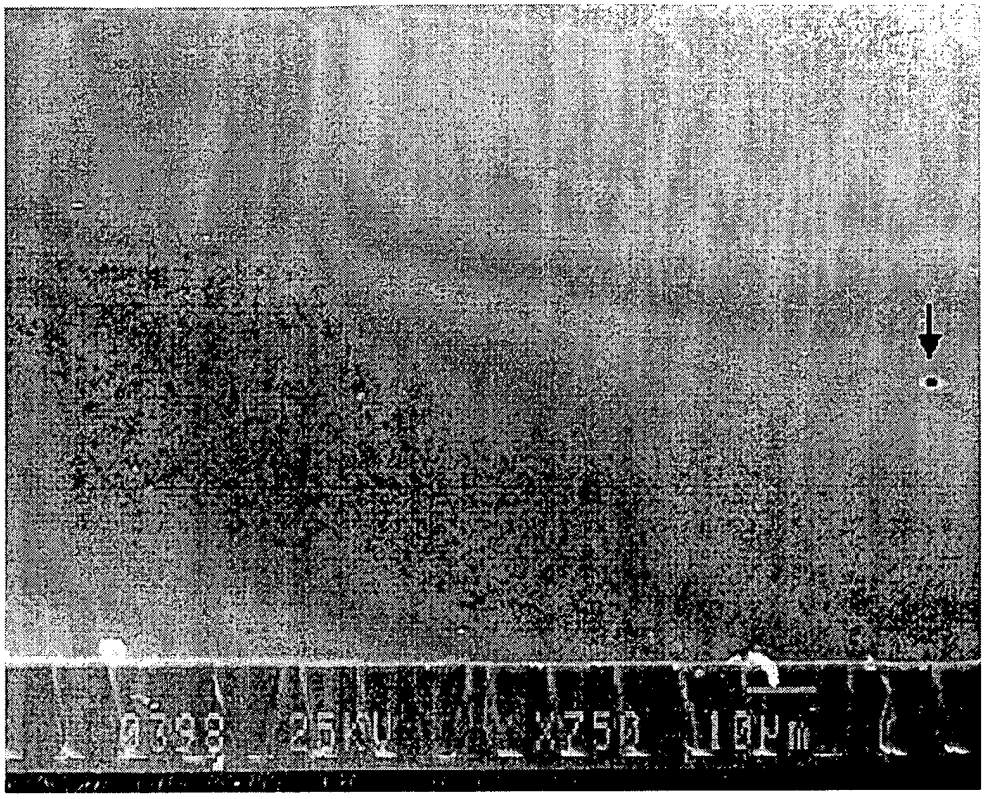

Figure 11. SEM tilted view of the cross section, perpendicular to the stripes direction, of GaN overgrown using the two steps process on patterned GaN/Saphir substrate. Very smooth surfaces are obtained. The arrow points to an hexagonal pit formed at the coalescence boundary. Along the cross section a periodic grating of voids is seen.

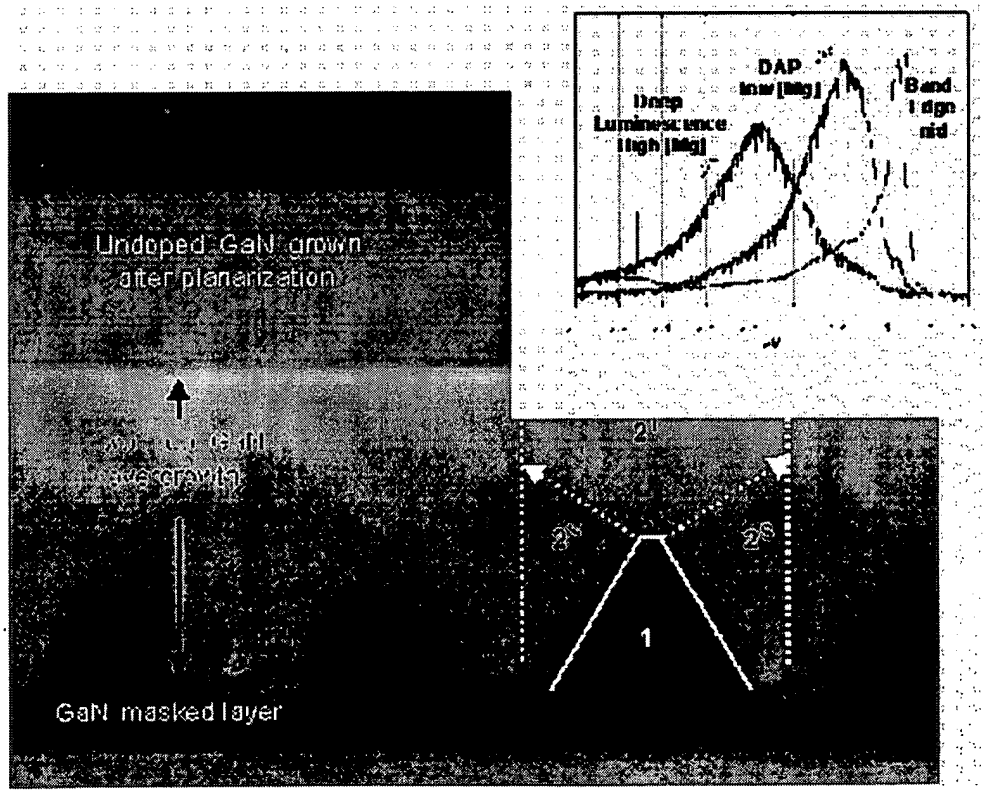

Figure 12. SEM cross section of two-step GaN overgrowth on GaN masked layer observed without

metallization at low temperature. Dashed vertical white lines are the coalescence boundaries. Plain white lines localize the border between steps 1 and 2. The volume filled during step 2 appears to be inhomogeneous, the volume labeled 2^S and 2^T are filled by expansion of the slants and the top C facets respectively. This is confirmed by cathodoluminescence spectra plotted in the inset. Volume 1 has a typical spectrum of undoped GaN whereas spectra of the volumes 2^S and 2^T correspond to GaN with low and high concentration of Mg respectively.

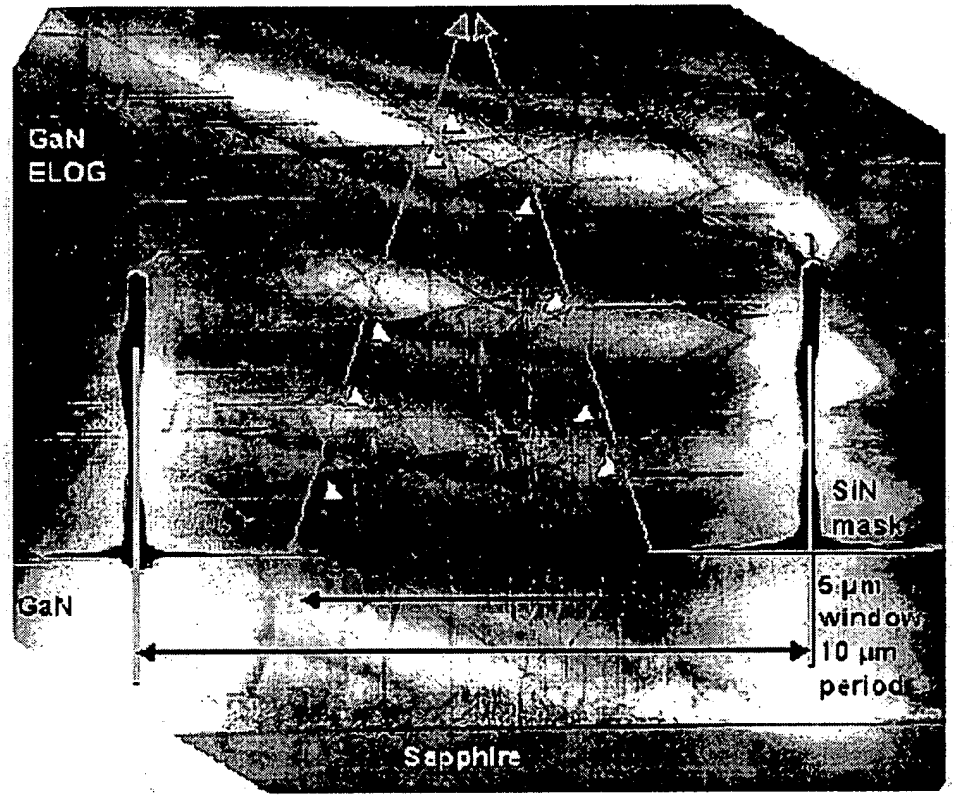

Figure 13. TEM cross section view of GaN overgrown with the two-step process.

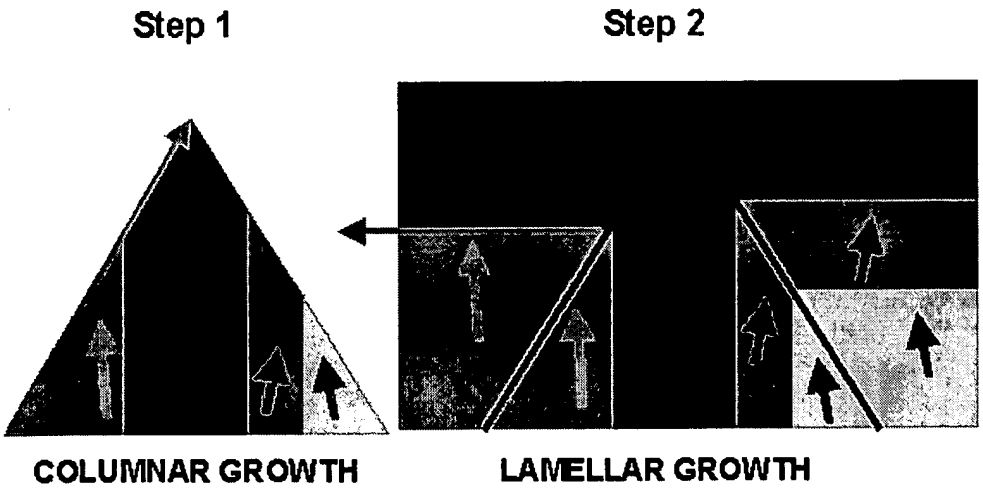

Figure 14. Schematic view of the two-step process. At the end of step 1 with essentially no lateral expansion, the template for the next growth step is formed by section of the misoriented columns by the slants. During step 2 where anisotropy force mainly lateral expansion, the misorientation of the

template could be replicated in stacked lamellae.

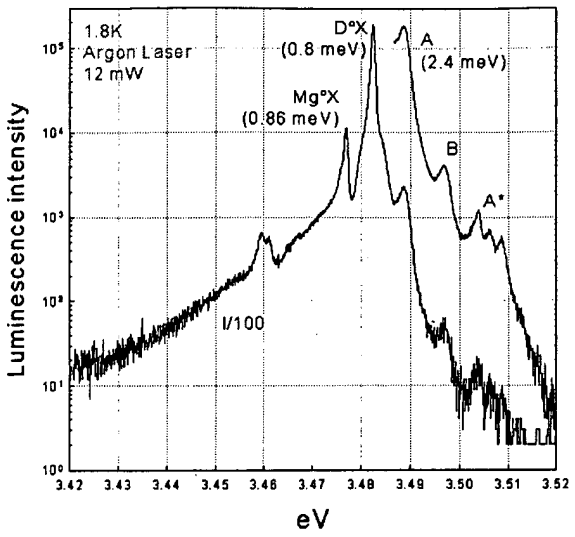

Figure 15. Low temperature luminescence spectrum measured on undoped GaN grown on top of a pseudo GaN substrate obtained by the to two-step overgrowth process. Bound excitons give very sharp (FWHM<1 meV) and intense peaks. Free exciton A, B and lines attributed to excited states of A are resolved.

Metal-organic vapor phase epitaxial growth of high-quality ZnO films on $Al_2O_3(00\cdot1)$

W.I. Park, S-J. An, Gyu-Chul Yi,[a] and Hyun M. Jang
Department of Materials Science and Engineering, Pohang University of Science and Technology (POSTECH), Pohang 790–784, Korea

(Received 6 September 2000; accepted 20 February 2001)

High-quality ZnO thin films were grown epitaxially at 250–550 °C $Al_2O_3(00\cdot1)$ substrates using low-pressure metalorganic vapor phase epitaxy. The reactants for the growth were diethylzinc and oxygen. Growth temperature, one of the important experimental parameters for epitaxial layers, was optimized. The films grown at 500 °C exhibited good crystallinity and strong ultraviolet absorption and emission. Photoluminescence spectra of the films showed a dominant excitonic emission with a weak deep level emission. More importantly, a strong stimulated emission peak was observed even at room temperature.

I. INTRODUCTION

Much attention has been paid recently to ZnO for short-wavelength photonic device applications since it has a direct band gap energy of 3.3 eV at room temperature.[1] Due to its large exciton binding energy of 60 meV,[2] ZnO has demonstrated strong excitonic emission in the ultraviolet (UV) range even at room temperature.[3] The exciton binding energy is twice as large as that of GaN, the most popular material for blue lasers. In addition, the band gap energy of ZnO can be extended to 4 eV by adding Mg or Mn and narrowed to 2.8 eV by alloying with CdO.[4] Furthermore, ZnO can be grown at 500 °C, hundreds of degrees lower than gallium nitride, which enables the growth of ZnO on Si and glass substrates.[5]

For ZnO film growth, numerous deposition techniques including sputtering, pulsed laser deposition (PLD), molecular beam epitaxy (MBE), and metalorganic vapor phase epitaxy (MOVPE) have been employed.[6–8] Among these techniques, MBE has yielded high quality ZnO epilayers which have shown good crystallinity and strong room-temperature excitonic emission.[3,7] Meanwhile, stimulated emission from MOVPE-grown ZnO has not yet been reported, which may result from the difficulty in growing high-quality ZnO films by MOVPE. This contrasts with the successful MOVPE growth of high-quality GaN and its alloys.[9] In the MOVPE of ZnO films, the films have been generally grown by chemical reaction between dimethylzinc (DMZn) or diethylzinc (DEZn) and O_2 or H_2O.[10] However, the Zn precursors are highly reactive with oxygen and water vapor so that pre-reaction in the gas phase occurs easily, resulting in the formation of white powders and degradation of film quality.[11] In this research, the pre-reaction was significantly reduced since the films were grown at low pressure in a cold-wall reactor with two separate inlets for the reactant. Using this MOVPE growth technique, high-quality ZnO films were grown on $Al_2O_3(00\cdot1)$ substrates as determined by x-ray diffraction and optical characterization.

II. EXPERIMENTAL PROCEDURE

The ZnO layers were grown on $Al_2O_3(00\cdot1)$ substrates using a horizontal-type MOVPE system. For the film growth, DEZn and oxygen were employed as the reactants, and argon as the carrier gas. The flow rates of oxygen and DEZn used were in the range of 20–50 sccm and 1–5 sccm at a bubbler temperature of 10 °C, respectively. The growth temperature investigated in this research ranged from 250 to 550 °C. To prevent premature reaction of the reactants, the O_2 gas line was separated from the main gas manifold line, and the pressure in the reactor during growth was kept at 5 torr.

Film thicknesses were measured using both surface profilometry and cross-sectional scanning electron microscopy. For surface profilometry measurements, ZnO layers were deposited with a thin substrate fragment placed on the substrate corner. The typical thickness of the films grown for 1 h was 1–1.5 μm.

As-grown ZnO films were highly transparent and specular. For optical characterization of the films, UV transmission and photoluminescence (PL) techniques were employed. The transmission of the films was measured with a two-beam spectrometer. Prior to the

[a]Address all correspondence to this author.
e-mail: gcyi@postech.ac.kr

measurements, a background correction was performed over the optical scan range of 300 to 1200 nm. The transmission spectra of the films were obtained by subtracting substrate spectra from the film/substrate spectra.

PL measurements were performed using a pulsed nitrogen laser (337 nm) or a continuous wave (cw). He–Cd laser (325 nm) as the excitation source. Film luminescence was measured with a detection system equipped with a photomultiplier and a photon counter. For the spectroscopic measurements, both the detection system and a grating monochromator were computer controlled. A typical scan range was 2.0–3.5 eV with an instrumental resolution of 0.1 nm. For low-temperature measurements, the samples were cooled with a He Displex system.

III. RESULTS AND DISCUSSION

The crystal structure and film orientation of the as-grown films were investigated using Θ–2Θ scans of x-ray diffractometry (XRD). Typically, ZnO films grown at 250–550 °C were epitaxially grown on Al_2O_3(00·1). As shown in Fig. 1, the XRD data of ZnO films exhibited a 2Θ peak at 34.47°, which corresponds to the (00·2) peak of ZnO. Figure 1 also indicates that the crystallization temperature of ZnO films was as low as 250 °C.

X-ray rocking curve measurements were carried out to determine the degree of film alignment perpendicular to the substrate. Figure 2(a) shows a typical XRD rocking curve of as-deposited ZnO films grown at 500 °C. The rocking curve was measured at the (00·2) reflection of the ZnO films. As shown in Figure 2(a), an XRD rocking curve of ZnO grown at 500 °C exhibits a full width at half-maximum (FWHM) of 0.19°, which indicates high crystallinity of the ZnO film. The FWHM value is narrower than the previous value of 0.25° of MOVPE-grown ZnO on an *r*-plane sapphire substrate.[11]

The degree of in-plane alignment in the films was further examined using XRD pole figure analysis. A ZnO crystal with a *c*-axis orientation possesses 6-fold symmetry. Thus, six poles should appear in the pole figure if it has a homogeneous in-plane alignment. As presented in Fig. 2(b), the six poles, separated one from another by 60°, are evident in the pole figure of the ZnO film. The 60° rotational symmetry clearly indicates that the ZnO film was grown epitaxially with homogeneous in-plane alignment.

Growth temperature is one of the most important parameters in the growth of high-quality epitaxial films. The effect of growth temperature on the crystallinity of ZnO films was investigated using XRD rocking curve measurements. As shown in Fig. 3, growth temperature up to 500 °C resulted in decreasing the rocking curve

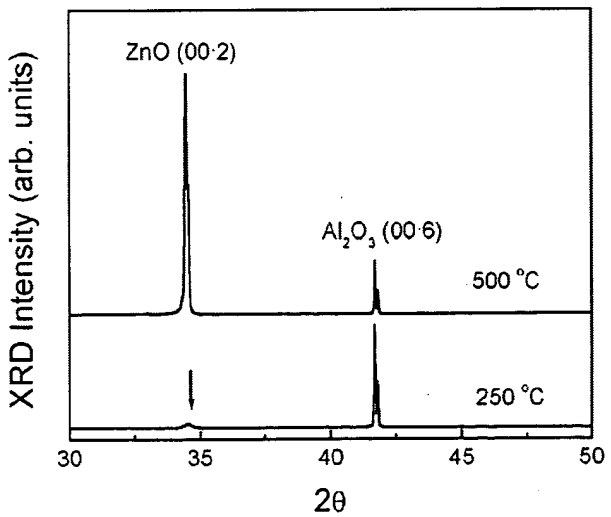

FIG. 1. 1. XRD Θ–2Θ scan results of ZnO films grown at 250 and 500 °C. The XRD data exhibits a 2Θ peak at 34.47°, which corresponds to the (00·2) peak of ZnO.

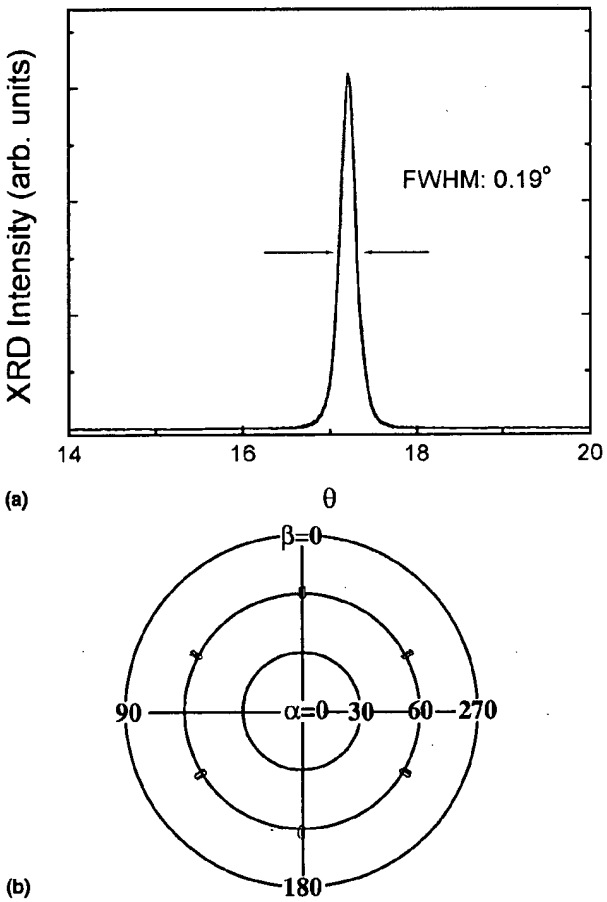

FIG. 2. (a) Typical x-ray rocking curve and (b) pole figure of a ZnO film grown on Al_2O_3(0001) at 500 °C using MOVPE. The ZnO film shows a narrow FWHM and 6-fold symmetry.

FWHM values. This indicates that films grown at higher growth temperatures up to 500 °C show better alignment along the *c* axis.

UV transmission measurements were carried out for optical characterization of the films. The optical absorbance was obtained from the optical transmittance of the ZnO films grown on double-side polished Al_2O_3 (00·1) substrates. Figure 4 shows the spectral dependence of the absorbance, which indicates low optical absorption in the visible region. The absorbance in the UV region increased abruptly near 3.2–3.3 eV, resulting from a band-to-band transition. In this transition, UV absorption occurs due to the excitation of electrons from the filled valence band to the conduction band.

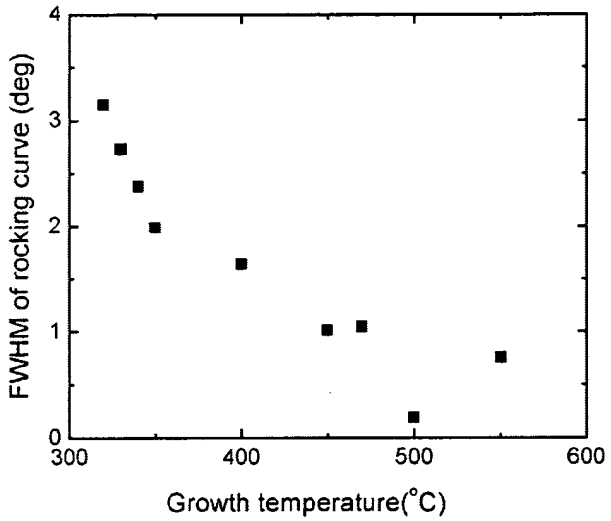

FIG. 3. XRD rocking curve results of ZnO films grown at different temperatures. The FWHM of the rocking curves decreases with increasing the growth temperature up to 500 °C.

Based on the UV absorbance measurements, the band gap energy of the films was calculated from the spectral dependence of the absorbance. By plotting $\alpha^2 E^2$ versus. E (α: absorbance, E: incident photon energy) and extrapolating the linear position of the curves to plotting $\alpha^2 E^2 = 0$, the band gap of the films is 3.24 eV, similar to the value of 3.2 eV previously reported by Kumar *et al.*[12]

Figure 5 shows a typical low temperature PL spectrum measured at 15 K. The 325 nm line of a He–Cd laser was used to illuminate the ZnO films grown at 500 °C. As shown in Fig. 5, the dominant emission peak of the ZnO film was observed at 3.364 eV, which is tentatively attributed to the exciton transition (I_2) bound to neutral donors. Narrow emission due to the excitons was usually observed in the low-temperature PL spectra of ZnO bulk crystals and MBE-grown films.[13,14] The exciton peak of the MOVPE-grown film showed a FWHM value of 7 meV, comparable to 6 meV (11 K) from ZnO grown on *r*-Al_2O_3, 1.5 meV (2 K) from bulk ZnO, and 8.9 meV (4.2K) from ZnO grown on GaN/SiC.[11,13,14]

In addition to the dominant exciton peak, a deep level emission band centered at 2.0 eV was also observed as indicated by an arrow in Fig. 5. The origin of the deep level emission is not yet clearly identified but it is presumably associated with structural defects or impurities. As shown in Fig. 5, the present MOVPE-grown film exhibited extremely weak deep level emission. The

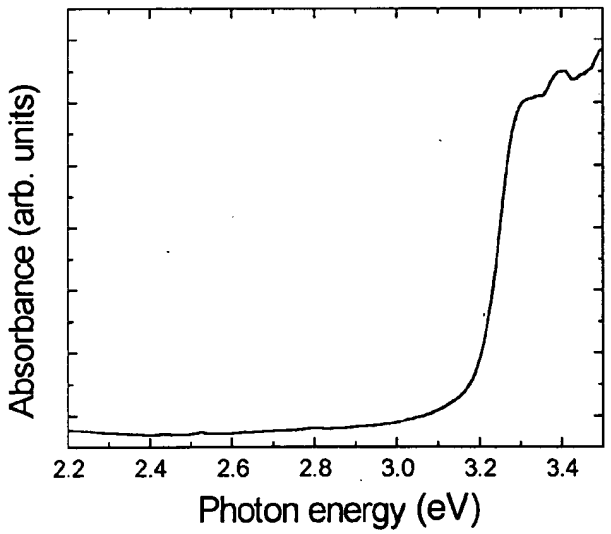

FIG. 4. Room-temperature absorbance spectrum of ZnO. The absorbance spectrum shows a low absorbance in the visible region and strong UV absorption at 3.2–3.3 eV.

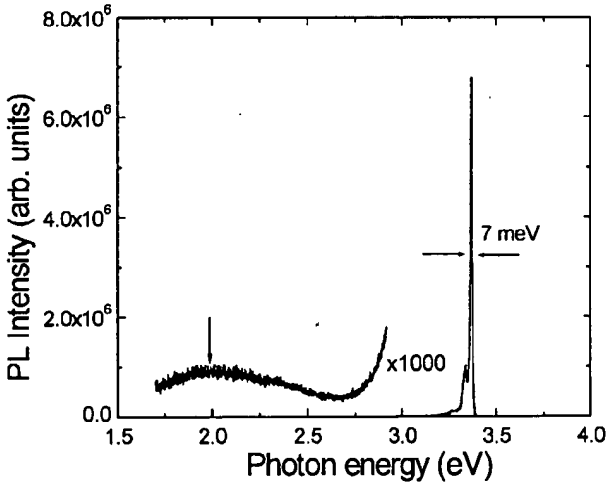

FIG. 5. PL spectrum of ZnO at 15 K. The PL spectrum was measured at 15 K using the 325 nm line of a He–Cd laser. A dominant emission peak was observed at 3.364 eV with a very weak deep level emission at 2.0 eV as indicated by an arrow. The near-band-edge emission is tentatively attributed to a neutral donor-bound exciton peak.

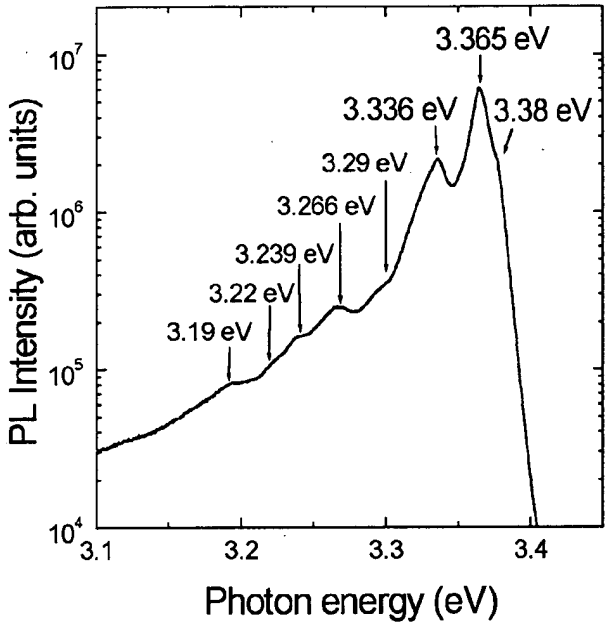

FIG. 6. High-resolution PL spectrum at 15 K. The PL spectrum shows five apparent peaks at 3.365, 3.336, 3.266, 3.239, and 3.192 eV and three shoulders at 3.38, 3.29, and 3.22 eV.

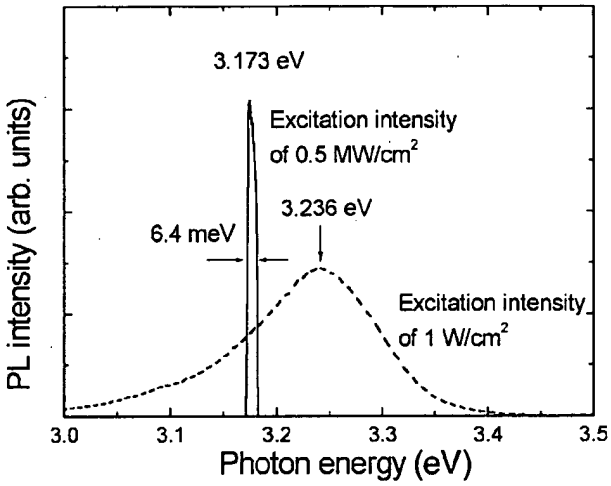

FIG. 7. Room-temperature PL spectra of ZnO grown at 500 °C. The PL spectra were measured using different excitation intensities of 1 W/cm² and 0.5 MW/cm². A broad peak was observed at 3.236 eV for the low excitation intensity. For the high excitation intensity of 0.5 MW/cm², however, a strong and narrow emission was observed at 3.173 eV.

intensity ratio of band-edge emission to deep level emission is about 6700, while ZnO grown by MBE has a ratio of around 100–500.[15] The sharp excitonic emission and weak deep level emission indicate that the MOVPE-grown film is of high quality.

High-resolution PL spectra were measured to determine the origin of the near-band-edge (NBE) emission. As shown in Figure 6, it is evident that the NBE emission at 15 K is composed of five apparent peaks at 3.365, 3.336, 3.266, 3.239, and 3.192 eV and three shoulders at 3.38, 3.29, and 3.22 eV. The dominant peak at 3.365 eV is tentatively ascribed to the exciton transition (I_2) bound to neutral donors since a similar peak has been observed at 3.365, 3.363, 3.36, and 3.360 eV for bulk single crystals and MOCVD, PLD, MBE-grown films, respectively.[6,11,13,15] Another peak at 3.336 eV is tentatively attributed to the exciton transition bound to neutral acceptors or deep donors. Compared with the previous report, the weak shoulder at 3.38 eV is presumably due to a transition from free excitons.[6,15]

Meanwhile several weak peaks and shoulders are also observed at 3.1–3.3 eV. In particular, they have a regular interval of 72 ± 2 meV, which almost coincides with the theoretical value calculated by Klingshirn.[16] Hence, the shoulders at 3.29 and 3.22 eV might be longitudinal optical phonon replicas of the bound exciton peak at 3.365 eV, and the peaks at 3.266 and 3.192 eV are tentatively attributed to longitudinal optical phonon replicas of the bound exciton peak at 3.336 eV. The shoulder at 3.29 eV is due to the free exciton peak at 3.38 eV.

Figure 7 shows typical room-temperature PL spectra of MOVPE-grown ZnO, which were measured using different excitation sources of a cw He–Cd laser (a 325-nm line with an excitation intensity of 1 W/cm²) and a pulsed nitrogen laser (a 337 nm line with an excitation intensity of 0.5 MW/cm²). As shown in Fig. 7, a broad peak was observed at 3.236 eV when the 325-nm line with a low excitation intensity of 1 W/cm² illuminated the films. For the high excitation intensity of 0.5 MW/cm², however, a strong and narrow emission was observed at 3.173 eV. The FWHM of the emission is 6–7 meV. Since a similar peak was observed at 3.175–3.181 eV from MBE-grown films, the peak is tentatively attributed to the exciton-exciton scattering process.[3] To our knowledge, this is the first observation of stimulated emission from MOVPE-grown ZnO. The strong excitonic emission from the MOVPE-grown ZnO film strongly suggests that MOVPE can be used to grown high-quality epitaxial ZnO films for highly efficient light emitters.

IV. CONCLUSIONS

In conclusion, high-quality ZnO thin films were grown on Al_2O_3(00·1) substrates using low-pressure MOVPE. Films grown at the optimized growth temperature of 500 °C showed strong UV absorption at 3.22–3.24 eV and a dominant excitonic emission at room temperature. From the PL spectra measured at 15 K, a dominant PL emission peak was observed at 3.364 eV with a FWHM of 7 meV. More importantly, room-temperature PL

spectra measured with an excitation intensity of 0.5 MW/cm^2 exhibited a strong stimulated emission peak at 3.173 eV with a FWHM of 6 meV.

ACKNOWLEDGMENTS

This research was sponsored by POSTECH BSRI Special Fund-2000, the Brain Korea 21 project, and the KISTEP through the National Research Laboratory program. Extensive use of the facilities at POSTECH is acknowledged.

REFERENCES

1. R.F. Service, Science **276,** 895 (1997).
2. W.Y. Liang and A.D. Yoffe, Phys. Rev. Lett. **20,** 59 (1968).
3. P. Zu, Z.K. Tang, G.K.L. Wong, M. Kawasaki, A. Ohtomo, H. Koinuma, and Y. Segawa, Solid State Commun. **103,** 459 (1997).
4. T. Fukumura, Z. Jin, A. Ohtomo, H. Koinuma, and M. Kawasaki, Appl. Phys. Lett. **75,** 3366 (1999).
5. W.I. Park and G-C. Yi (unpublished).
6. R.D. Vispute, V. Talyansky, S. Choopun, R.P. Sharma, T. Venkatesan, M. He, X. Tang, J.B. Halpern, M.G. Spencer, Y.X. Li, L.G. Salamanca-Riba, A.A. Iliadis, and K.A. Jones. Appl. Phys. Lett. **73,** 348 (1998).
7. D.M. Bagnall, Y.F. Chen, Z. Zhu, T. Yao, M.Y. Shen, and T. Goto, Appl. Phys. Lett. **73,** 1038 (1998).
8. P. Souletie and B.W. Wessels, J. Mater. Res. **3,** 740 (1988).
9. S. Nakamura, Jpn. J. Appl. Phys. **30,** L1705 (1991).
10. S.K. Ghandhi, R.J. Field, and J.R. Shealy, Appl. Phys. Lett. **37,** 449 (1980).
11. C.R. Gorla, N.W. Emanetoglu, S. Liang, W.E. Mayo, Y. Lu, M. Wraback, and H. Shen, J. Appl. Phys. **85,** 2595 (1999); N.W. Emanetoglu, C. Gorla, Y. Liu, S. Liang, and Y. Lu, Mater. Sci. Semicon. Process. **2,** 247 (1999).
12. N.D. Kumar, M.N. Kamalasanan, and S. Chandra, Appl. Phys. Lett. **65,** 1373 (1994).
13. D.C. Look, D.C. Reynolds, J.R. Sizelove, R.L. Jones, C.W. Litton, G. Cantwell, and W.C. Harsch, Solid State Commun. **105,** 399 (1998).
14. M.A.L. Johnson, S. Fujita, W.H. Rowland, Jr., W.C. Huges, J. W. Cook, Jr., and J.F. Schetzina, J. Electron. Mater. **25,** 855 (1996).
15. D.M. Bagnall, Y.F. Chen, M.Y. Shen, Z. Zhu, T. Goto, and T. Yao, J. Cryst. Growth. **184/185,** 605 (1998); Y. Chen, D. Bagnall, and T. Yao, Mater. Sci. Eng. B **75,** 190 (2000).
16. C. Klingshirn, Phys. Status Solidi B **71,** 547 (1975).

SOL-GEL SCIENCE

The Physics and Chemistry of Sol-Gel Processing

C. Jeffrey Brinker

Sandia National Laboratories
Albuquerque, New Mexico

George W. Scherer

E. I. du Pont de Nemours & Company
Wilmington, Delaware

Academic Press
San Diego New York Boston
London Sydney Tokyo Toronto

Find Us on the Web! http://www.apnet.com

This book is printed on acid-free paper. ♾

ACADEMIC PRESS
A Division of Harcourt Brace & Company
525 B Street, Suite 1900, San Diego, California 92101-4495

United Kingdom Edition published by
ACADEMIC PRESS LIMITED.
24-28 Oval Road, London NW1 7DX

Library of Congress Cataloging-in-Publication Data

Brinker, C. Jeffrey.
Sol-gel science : the physics and chemistry of sol-gel processing / C. Jeffrey Brinker, George W. Scherer.
p. cm.
Includes bibliographical references.
ISBN 0-12-134970-5 (alk. paper)
1. Ceramic materials. 2. Colloids. I. Scherer, George W. II. Title.
TP810.5.B75 1990
666—dc20 89-15631
CIP

Printed in the United States of America
98 99 00 01 02 EB 12 11 10 9 8

1. SOL-GEL PROCESSING

A *colloid* is a suspension in which the dispersed phase is so small (~1–1000 nm) that gravitational forces are negligible and interactions are dominated by short-range forces, such as van der Waals attraction and surface charges. The inertia of the dispersed phase is small enough that it exhibits *Brownian motion* (or *Brownian diffusion*), a random walk driven by momentum imparted by collisions with molecules of the suspending medium. A *sol* is a colloidal suspension of solid particles in a liquid. An *aerosol* is a colloidal suspension of particles in a gas (the suspension may be called a *fog* if the particles are liquid and a *smoke* if they are solid) and an *emulsion* is a suspension of liquid droplets in another liquid. All of these types of colloids can be used to generate polymers or particles from which ceramic materials can be made. A *ceramic* is usually defined by saying what it is *not*: it is nonmetallic and inorganic; some would also say it is not a chalcogenide. We thus include all metal oxides, nitrides, and carbides, both crystalline and noncrystalline. In the sol-gel process, the *precursors* (starting compounds) for preparation of a colloid consist of a metal or metalloid element surrounded by various *ligands* (appendages *not* including another metal or metalloid atom). For example, common precursors for aluminum oxide include *inorganic* (containing no carbon) salts such as $Al(NO_3)_3$ and *organic* compounds such as $Al(OC_4H_9)_3$. The latter is an example of an *alkoxide*, the class of precursors most widely used in sol-gel research. An *alkane* is a molecule containing only carbon and hydrogen linked exclusively by single bonds, as in *methane* (CH_4) and *ethane* (C_2H_6); the general formula is C_nH_{2n+2}. An *alkyl* is a ligand formed by removing one hydrogen (proton) from an alkane molecule producing, for example, *methyl* ($\bullet CH_3$) or *ethyl* ($\bullet C_2H_5$) (where the dot $\bullet$ indicates an electron that is available to form a bond). An *alcohol* is a molecule formed by adding a *hydroxyl* (OH) group to an alkyl (or other) molecule, as in *methanol* (CH_3OH) or *ethanol* (C_2H_5OH). An *alkoxy* is a ligand formed by removing a proton from the hydroxyl on an alcohol, as in *methoxy* ($\bullet OCH_3$) or *ethoxy* ($\bullet OC_2H_5$). A list of the most commonly used alkoxy ligands is presented in Table 1.

Metal alkoxides are members of the family of *metalorganic* compounds, which have an organic ligand attached to a metal or metalloid atom. The most thoroughly studied example is silicon tetraethoxide (or tetraethoxysilane, or tetraethyl orthosilicate, TEOS), $Si(OC_2H_5)_4$. *Organometallic* compounds are defined as having direct metal–carbon bonds, not metal–oxygen–carbon linkages as in metal alkoxides; thus, alkoxides are not organometallic compounds, although that usage turns up frequently in the

IN THE UNITED STATES PATENT AND TRADEMARK OFFICE

Applicant(s):	Richard N. Zare		
Title:	Photopolymerized Sol-Gel Column and Associated Methods		
Serial No.:	09/929,275	Filed:	August 13, 2001
Examiner:	Therkorn, Ernest G.	Group Art Unit:	1723
Docket No.:	STNB.066US0	Conf. No.:	8199

Mail Stop AF
Commissioner for Patents
P.O. Box 1450
Alexandria, VA 22313-1450

DECLARATION OF MARIA T. DULAY

I, Maria T. Dulay, declare under penalty of perjury as set forth below.

1. I am one of the named inventors in the above-identified patent application ("Application") and am an employee of The Board of Trustees of The Leland Stanford Junior University, the assignee ("Assignee") of the Application. I earned a B.A. in Chemistry (*Cum Laude*) from Mount Holyoke College in 1988 and a Ph.D. in Physical Chemistry from The University of Texas at Austin in 1993. I have worked for the Assignee from 1993 to 1996 as a Postdoctoral Research Associate, National Institutes of Health Fellow, and from 1997 to the present as a Research Scientist.

2. I understand that Claims 53-60, as they appear in Exhibit 1 hereto, are now pending in the Application.

3. I have read the Office Action ("Office Action") that issued in the Application and bears a mailing date of January 22, 2004, and understand the content thereof.

4. I am one of the authors of the article of Dulay *et al.*, *Preparation and Characterization of Monolithic Porous Capillary Columns Loaded with Chromatographic Particles*, Anal. Chem., Vol. 70, No. 23 (1998), 5103-5107 (hereinafter, "Dulay"), and am very familiar with and very well understand the content of Dulay.

5. I have read the article of Viklund *et al.*, *"Molded" Macroporous Poly(glycidyl methacrylate-co-trimethylolpropane trimethacrylate) Materials with Fine Controlled Porous Properties: Preparation of Monoliths Using Photoinitiated Polymerization*, Chem. Mater., Vol. 9 (1997), 463-471 (hereinafter, "Viklund"), and understand the content of Viklund.

6. I understand Dulay as teaching a starting mixture of tetraethyl orthosilicate (TEOS), ethanol, and a dilute HCl solution to acidify the mixture. I understand this teaching of Dulay as referring to ethanol as an agent for solubilizing the TEOS, as TEOS is not freely soluble in water, not as a reactive agent. I understand this teaching of Dulay as referring to a hydrolysis reaction, in which the ethanol does not participate, that results in the formation of an inorganic $Si(OH)_4$ product and ethanol. I understand Dulay as teaching, by virtue of the amount of HCl and water in the starting mixture, that the hydrolysis reaction goes to completion, such that the TEOS is fully converted to the inorganic $Si(OH)_4$ product and ethanol. I do not read Dulay as teaching or suggesting that the inorganic $Si(OH)_4$ product or the ethanol in the resulting mixture is a metal organic compound, and I do not understand inorganic $Si(OH)_4$ or ethanol as being a metal organic compound.

7. I understand Dulay as teaching that the above-mentioned resulting mixture has no chromatographic capability, and understand this resulting mixture as having no chromatographic capability. I understand Dulay as teaching that a component that has chromatographic capability must be added to the resulting mixture to produce a column with chromatographic capability. I understand Dulay as teaching that various materials, namely, chromatographic octadecylsilica particles and bare silica, are added to the resulting mixture. I do not read Dulay as teaching or suggesting that the octadecylsilica particles react with any of the components in the resultant combination, and I do not understand that the octadecylsilica do so react.

8. I understand Dulay as teaching that the above-mentioned resultant combination is sonicated and then introduced into capillary columns, whereupon a filled column is placed on a hot plate and heated above 373 K for about 24 hours. I understand this teaching of Dulay as referring to the condensation of the inorganic $Si(OH)_4$ in the column filling, such that the inorganic $Si(OH)_4$ polymerizes and the ethanol evaporates until the column is dry. I do not read Dulay as teaching or suggesting that the inorganic $Si(OH)_4$ polymerization product is a metal organic compound, and I do not understand inorganic polymerized $Si(OH)_4$ as being a metal organic compound. I read Dulay as teaching that the octadecylsilica particles become embedded or trapped in the resulting inorganic sol-gel matrix, but do not become part of that

matrix itself, and I understand this to be the case. I do not read Dulay as teaching or suggesting that the resulting matrix comprises a metal organic polymer, and I do not understand that the resulting matrix comprises a metal organic polymer.

9. I understand that in the Office Action, it is alleged that the claims differ from Dulay in reciting irradiating the mixture. As to Claims 53-60, I read and understand these claims as differing from Dulay at least in reciting a method that comprises a combination of elements that includes providing a separation column, providing an initial mixture, as recited, such that a resulting mixture that results from the initial mixture comprises a metal organic compound, introducing the resulting mixture into the column, and irradiating the resulting mixture to form, via photoinitiated polymerization, a fritless, porous matrix comprising a metal organic polymer in the column, as recited, not merely in reciting irradiating the resulting mixture.

10. I understand Viklund as teaching preparing an initial mixture that comprises benzoin methyl ether initiator, glycidyl methacrylate, trimethylolpropane trimethacrylate, isooctane and toluene; purging that mixture with helium; and transferring the resulting mixture to a pre-treated quartz tube, whereupon the tube is sealed and irradiated. I do not read Viklund as teaching or suggesting that the above-mentioned initial mixture comprises a metal alkoxide, and I do not understand this initial mixture as comprising a metal alkoxide. I do not read Viklund as teaching or suggesting that the above-mentioned resulting mixture comprises a metal organic compound, and I do not understand this resulting mixture as comprising a metal organic compound. I do not read Viklund as teaching or suggesting that the ultimate monolith produced in the quartz tube comprises a metal organic polymer, and I do not understand the ultimate monolith of Viklund as comprising a metal organic polymer.

11. I understand that in the Office Action, it is alleged that it would have been obvious to use photoinitiated polymerization in Dulay because Viklund discloses various advantages of photoinitiated polymerization. I do not believe that Viklund would have been viewed as advantageous in terms of ease of preparation, in terms of time, or in terms of temperature, relative to Dulay. That is, I understand Viklund's procedures as being complicated and time-consuming relative to those of Dulay, as Viklund's procedures involve multiple involved and time-consuming steps, including an overnight preparation of monomers, an involved and time-consuming preparation of polymerization tubes that takes on the order of over 8 hours, preparation of a composition including the monomers and introduction of the composition into a column, and a polymerization procedure that takes over 2 hours, while Dulay's procedures involve a simple preparation of a composition and

introduction of the composition into a column, followed by an approximately 24-hour heating step. Further, I understand that Viklund's teaching regarding temperature is made relative to the preparation of imprinted matrixes for molecular recognition, not as to all preparations, and not as to Dulay.

12. While I do not believe it would have been obvious to use photoinitiated polymerization in Dulay, based on the teachings of Viklund, I understand that if it would have been possible, somehow, to use photoinitiated polymerization in Dulay, there would still be no porous matrix comprising a metal organic polymer in the column, as I do not understand Dulay or Viklund as teaching the presence of a porous matrix comprising a metal organic polymer in a column.

I further declare that all statements made herein of my knowledge are true and that all statements made on information and belief are believed to be true; and further that these statements were made with the knowledge that willful false statements and the like so made are punishable by fine or imprisonment, or both, under Section 1001 of Title 18 of the United States Code, and that such willful false statements may jeopardize the validity of the application or any patent issuing therefrom.

I hereby execute this declaration as set forth below.

Maria T. Dulay — June 22, 2004

Maria T. Dulay — Date

CLAIMS 53-60

53. (New) A method of preparing a porous matrix in a separation column, comprising:

providing a separation column;

providing an initial mixture of at least one porogen, at least one metal alkoxide, and at least one photoactive material selected from a group consisting of a photoactive group associated with the metal organic monomer, a photoinitiator, and any combination thereof, such that a resulting mixture that results from said initial mixture comprises a metal organic compound;

introducing the resulting mixture into the column; and

irradiating the resulting mixture to form, via photoinitiated polymerization, a fritless, porous matrix comprising a metal organic polymer in the column.

54. (New) The method of claim 53, wherein the matrix contains no chromatographic particles.

55. (New) The method of claim 53, wherein the photoactive group is a methacrylate.

56. (New) The method of claim 53, wherein the porogen is selected to controllably form pores in the matrix.

57. (New) The method of claim 53, further comprising selecting a molar ratio of monomer to porogen to form pores in the matrix.

58. (New) The method of claim 53, wherein the irradiating comprises irradiating the mixture with visible or ultraviolet light.

59. (New) The method of claim 53, further comprising, after the irradiating, introducing an organic solvent into the column.

60. (New) The method of claim 53, wherein the providing comprises providing a capillary or a planar structure.